University of Alberta

Wellbore Seismic and Core Sample Measurement Analysis:
Integrated Geophysical Study of The Lake Bosumtwi Impact Structure,
Ghana

by

Damien Meillieux

A thesis submitted to the Faculty of Graduate Studies and Research
in partial fulfillment of the requirements for the degree of

Master of Science

in

Geophysics

Department of Physics

©Damien Meillieux
Fall 2009
Edmonton, Alberta

Examining Committee

Douglas Schmitt, Physics

Mauricio Sacchi, Physics

James Pinfold, Physics

Christopher Herd, Earth and Atmospheric Sciences

Abstract

Wellbore seismic measurements were recorded in the Lake Bosumtwi impact structure, Ghana, in 2004. A full range of petrophysical measurements were also performed in the laboratory on core samples from the same boreholes.

The Vertical Seismic Profile shows low velocities for both P and S waves in the hardrock basement of the crater. Although we were expected to locate fractures within the rock, no upgoing waves were detected. Density and porosity measurements on the core samples indicate higher than normal porosity in the impact damaged rocks. Mercury porosimetry and SEM analysis characterized the pores as impact induced microcracks. These microcracks are most likely the reason for the low velocities observed on the seismic profiles, the in situ sonic logs, and the seismic velocity measurements on the core samples. Furthermore our laboratory P and S velocities measurements indicate a strong heterogeneity within the impactites.

Acknowledgment

Table of Contents

List of Figures

Authorization was granted from original publisher for figures reproduced with or without modification in the work presented here.

Glossary

Allochtonous: Used for a rock that was moved from its original location (by natural process).

Autochtonous: Used for a rock that still remains at the original location it was formed.

Ballen quartz: Quartz crystal displaying a texture typical and unique of impact events.

Breccia: Sedimentary rock constituted by many angular fragments (clasts) of preexisting rocks and newly formed cement. A breccia is monomict when all the fragments have the same lithology, and polymict when they differ.

Diaplectic glass: Glass formed out of a mineral phase without melting.

Impactite: Rock created by an impact event. Most common types are impact breccias and suevites.

Tektite: Small glassy spherical particle of rock molten and ejected by the energy of an impact event.

Metamorphism: Changes in the mineralogical composition of a rock under changing heat and pressure conditions.

Meteor: The light produced by friction when a meteoroid enters into the atmosphere with great speed. Commonly called a shooting star.

Meteoroid: Small (usually less than 1 km) natural object whose orbit around the sun may cause it to collide with other planetary bodies, like the Earth. (Lunar and Planetary Laboratory, 2009)

Planar Deformation Features: PDfs are optical anomalies in a mineral (usually quartz) observable with an optical microscope. They form only during impact events.

Seismic wave: Elastic wave propagating at the speed of sound (pressure or P wave) or slower (shear or S wave).

Shock wave: Supersonic and non-elastic wave created by a sudden and very energetic event, e.g. impact of a meteoroid on a solid material's surface.

Spallation: Ejection of fragments (spalls) from the surface of a solid material due to impact or tensile stress.

Suevite: Polymict breccia exhibiting some impact melts or glass particles. Suevite was first defined at the Ries impact crater, localized in the province of Swabia (Suavia in latin), southern Germany; hence its name (Dressler and Reimold, 2001).

Chapter 1

Introduction

The Earth, like other solid terrestrial planets, was formed by collision and accretion of planetoids. This sets impact cratering as a fundamental process in the formation of our solar system, our planet Earth, and the evolution of the Earth's crust. Yet this process had been considered to be only of marginal importance and hence ignored for a long time. Its primary importance in the evolution of our planet and of life has been increasingly acknowledged only in the last three decades. Scientific interest rose with geologists identifying more and more geologic structures on the surface of the Earth as impact craters (175 to date according to the Earth Impact Database, 2008), and with major discoveries showing the role of meteoroid impacts in the evolution of life on Earth (Alvarez et al., 1980), and lately in its genesis (Furukawa et al., 2009). As a consequence, impact structures have been targets of further geological and geophysical studies in the last two decades. Besides this obvious scientific interest lies also an economic one. The genesis of world-class mineralization provinces such as Sudbury in Canada or the Witwatersrand Basin in South Africa have been proved to be linked to huge impact events (Pati and Reimold, 2007), while smaller structures such as the Steen River in northern Alberta provide excellent traps for hydrocarbons (Donofrio, 1997).

Geological and geophysical signatures of impact craters have been widely studied and defined. Not much is known, however, about the physical damage of the target rocks induced by the impact event. This physical damage is mainly characterized by porosity introduced into the target rocks. And this porosity is of

primary importance since it allows for fluid circulation and storage, and is also the main petrophysical parameter controlling measurable quantities such as seismic velocities or electrical resistivity.

In 2004 the International Continental Scientific Drilling Program (ICDP) carried out an integrated drilling survey in the Bosumtwi Impact Structure, Ghana, including wireline loggings and Vertical Seismic Profiles (VSP), along with geological and geochemical studies. As a young crater Bosumtwi is well preserved and is expected to be typical for a small complex impact structure. Hence the data and core samples available provide a rare opportunity to examine the consequences of impact at many scales and to characterize the expected induced porosity.

Chapter 2

Impact Structures

2.1 Impacts on Earth

2.1.1 Resources in impact craters

The unique geological processes following an impact event may lead to the formation of rare minerals and rocks of significant economic interest. For example the Sudbury Basin in Canada, a 1.8 Ga old impact structure, is one of the oldest and biggest known terrestrial craters, and also one of the world's largest mineralization of nickel and copper. The accumulation of these elements is believed to be the direct result of the vast volume of rock shock melted during the impact event (Pati and Reimold, 2007). Post-impact hydrothermal fluid circulation in the impact damaged rocks is another process that may lead to significant mineralization. The world class gold mining basin of Witwatersrand in South Africa is probably the result of hot fluid circulation linked to the Vedrefort impact structure (Hayward et al., 2005), which is the biggest known on Earth (300 km in diameter). Another example is the much smaller Kärdla structure (4 km), Estonia, where the impact related origin of hydrothermal mineralization of metallic assemblages has been proven (Versh et al, 2003).

Impact craters can also represent good potential traps for hydrocarbons when buried below a suitable cap of sediments, due to the impact induced fracture porosity and fault traps. Some of them are actual oil producers, like Red Wing Creek in Dakota, USA, Avak in Alaska, USA, or Steen River in Alberta, Canada

(Donofrio, 1997).

2.1.2 Formation of craters and morphologies

The formation of a crater is usually subdivided into three stages (French, 1998). The first stage is the contact between the impactor (meteoroid) and the target rocks (Earth), and is usually called compression stage. At the end of this stage the impactor has totally disappeared, being vaporized or melted along with some of the superficial terrestrial material. At this stage a shock wave starts propagating into the target rocks.

The second stage is an outward excavation flow that climaxes with the formation of a bowl-shaped deep transient crater. During the formation of this crater, shallow rocks are pulverized or expelled into the atmosphere, while the shock wave and associated high strain propagate deeper and further into the target rock.

The third stage (or modification stage) is the inward collapse flow, where the transient crater refills to a large degree with the collapse of its now unstable walls. This phenomenon is probably helped by acoustic fluidization (Melosh, 1979). The final crater is hence much shallower than the transient cavity.

Depending on the size and on the nature of the target rocks, craters can be sorted out in two main different types. Simple craters are bowl-shaped features in which the final structure is close to the transient crater in shape (Figure 2.1). This is typical of small craters (diameter smaller than 4-5 km). Larger structures are called complex craters, and are characterized by a central uplift caused by the elastic rebound of the crater floor during the modification stage, and by the circular depression around it (Figure 2.2). For the largest complex craters, the central uplift displays a basin in its centre, and then is more like a central ring rather than a central peak. In crystalline target rocks, the transition diameter between simple and complex craters is around 5 km. The final observed crater is always shallower than the true crater, due to its fill with impactites (impact generated rocks) and melt rocks.

4
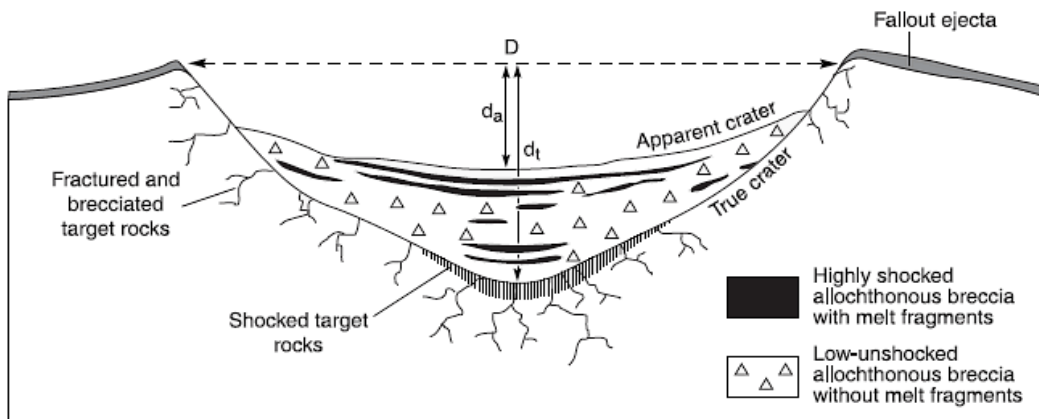
Figure 2.1: Cross section of a typical simple crater. D is the diameter, d_a the apparent depth of the crater, d_t the true depth. From French (1998).
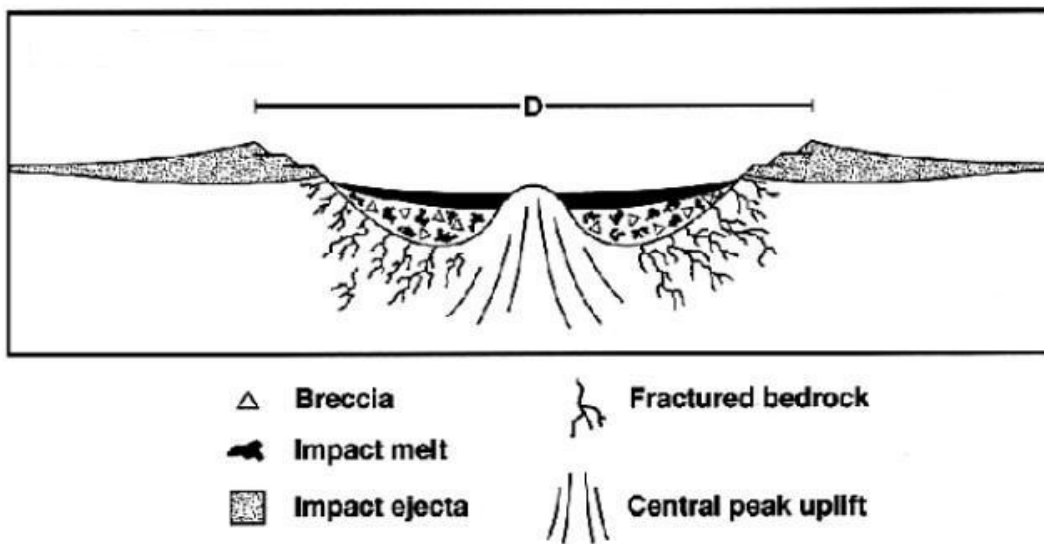
Figure 2.2: Cross section of a complex crater. D is the apparent diameter of the crater, from rim to rim. From Lunar & Planetary Institute (2008).

2.2   Shock effects on rocks and minerals

2.2.1   Physical damage at the rock scale

Shock waves generated by impacts are supersonic and non-elastic waves, while seismic waves that are used in geophysics are elastic with a sonic or subsonic velocity. Elastic means that the changes introduced into the medium the wave propagates through happen gradually and are reversible. They can be described by a continuous mathematical function. When these changes reach a critical intensity and velocity they are no longer continuous and reversible, they are discontinuous mathematically and irreversible: this is a shock wave (Figure 2.3). Hence elastic wave equations are no longer applicable and the Rankine-Hugoniot relations have to be used instead. Assuming the conservation of mass, momentum and energy across the wave front, we can write:

$$\sigma - \sigma_0 = \rho_0 (U_s - u_0)(u - u_0)$$

$$E - E_0 = \frac{1}{2}(\sigma + \sigma_0)\left(\frac{1}{\rho_0} - \frac{1}{\rho}\right)$$

The Rankine-Hugoniot equations establish a relationship between the stress σ, the density ρ, and the specific internal energy E on both sides of the wave front. U_s is the velocity of the shock wave front, u_0 and u are the particle velocity before and behind the wave front.

Shock waves are always compressive (i.e. $\sigma > \sigma_0$), which means that the change in energy ($E-E_0$) is always positive. This implies irreversible changes in physical parameters of the material, like a decrease of the density for example (Figure 2.4).

Shock waves introduce an intense and sudden deformation into the medium

they are propagating through. Rocks have to accommodate this strong deformation one way or another. Moderate strain (e.g. tectonic motions) can be accommodated through plastic (or ductile) deformation, i.e. the rock is squeezed by the wave and remains so. Higher degree strain (e.g. meteoroid impact) has to be accommodated through brittle deformation as well, i.e. in addition of plastic deformation the rock will break down into pieces or even be comminuted. An impact shock wave (always compressive) is immediately followed by a rarefaction wave that induces a tensile stress able to cause further damage to the rocks through different mechanisms such as spallation.

During the first and second stages of the formation of an impact crater the shock wave and associated strain are propagating into the target rock. Modeling by Collins et al. (2004) as well as laboratory experiments by Ai and Ahrens (2007) show that the strain is both due to shear failure caused by the primary shock wave and tensile failure caused by the following rarefaction wave. During the modification stage an additional tensile stress occurs beneath complex crater due to the elastic rebound that will form the central uplift. The main consequence of these strains in brittle materials such as rocks is the formation of cracks, i.e. porosity. This impact induced damage decreases very quickly and in a non-linear fashion with distance from the crater (Figure 2.5). Shock waves have the characteristic of losing their energy rapidly, and they eventually become regular seismic waves.

2.2.2 Shock metamorphic effects on minerals

Numerous permanent effects of the passage of the shock wave are also seen on minerals. The most common effects can be used as a barometer for the shock pressure and help to define progressive stages of shock metamorphism (French, 1998):

– Weakly shocked (shock pressure below 10 GPa and postshock temperature below 100 °C). Quartz and feldspars show planar fractures and micas show

kink bands. These effects can also be seen in the case of very strong tectonic stresses.

– Moderately shocked, (shock pressure up to 40 GPa and postshock temperature up to 300 °C). Quartz exhibit PDFs (Planar Deformation Features), which are the result of the deformation of the mineral lattice. Minerals transform to diaplectic glasses or to very high pressure polymorphs (coesite and stishovite for quartz). Such effects can be obtained only during impact events, that is, a true shock wave is required.

– Strongly shocked (shock pressure up to 60 GPa, temperature up to 1,500 °C). Some minerals start to melt.

– Very strongly shocked (shock pressure above 70 GPa and temperature above 2,000 °C). The whole rock is melted by the shock wave.

Ballen quartz is another signature feature of impact structure. Not much is known about this texture which is probably the result of shock melt followed by recrystallization or diaplectic transformations. Ballen quartz have been observed in several craters within a very large range of impact pressure (10 to 55 GPa, Pati et al., 2006).

2.2.3 Shock generated rocks

The energy of the impact can affect the target rocks to such a degree that new rocks will actually be formed. Though these rocks are broadly named impactites, we can distinguish several types (although these definitions may vary from one author to another).

Impact breccias are breccias containing lithic and mineral clasts excavated from the target rock. They deposit in or around the crater, or can be injected as dykes into the original target rocks. They are called monomict when there is one single source for all the clasts and polymict when several rock types are seen among clasts. Monomict breccias are often grading to unbrecciated but shattered

rock, and hence are considered as autochtonous breccias. Polymict breccias are often interpreted as allochtonous, due to the various origins of the clasts.

Suevites are polymict breccias exhibiting some impact melts or glass particles. They were first defined at the long studied Ries crater in southern Germany.

Other noticeable objects generated by impacts are tektites and microtektites. These are small particles of glass formed through the melting of target rocks and dispersed by the force of the impact, sometimes over thousands of square kilometers (Foucault et Raoult, 1995).

2.3 Motivation for the present work

The bulk of research about impact events has mainly focused on the formation of impact structures and on their general effects, such as rock melting or shock metamorphism in minerals. From a geophysical point of view, observed anomalies (gravimetric, magnetic, electrical, seismic) have been well characterized but often poorly explained. For example magnetic anomalies are attributed to magnetic melt material, but this has been very seldom found in craters. Another example is the low seismic velocities. While they are intuitively explained by impact induced porosity, this porosity itself has never been studied on natural impactites (work on "in the lab" impacted rocks has been achieved by Ai and Ahrens, 2004, and Liu and Arhens, 1997). A better understanding of these geophysical anomalies can be achieved through the study of the physical properties of the rocks. The most important parameter in this regard is porosity, since other parameters such as density or seismic velocity are depending on it. Porosity also allows for heated fluid circulation hundreds of years after the event and for potential storage of fluids. Hence measuring porosity, its distribution, the size and shape of the pores, is a key to understanding the evolution of the impact structure after its formation as well as the formation of potential economical resources. Very few studies have been achieved in this domain up to now, and that is what we are trying to do in the work presented here.
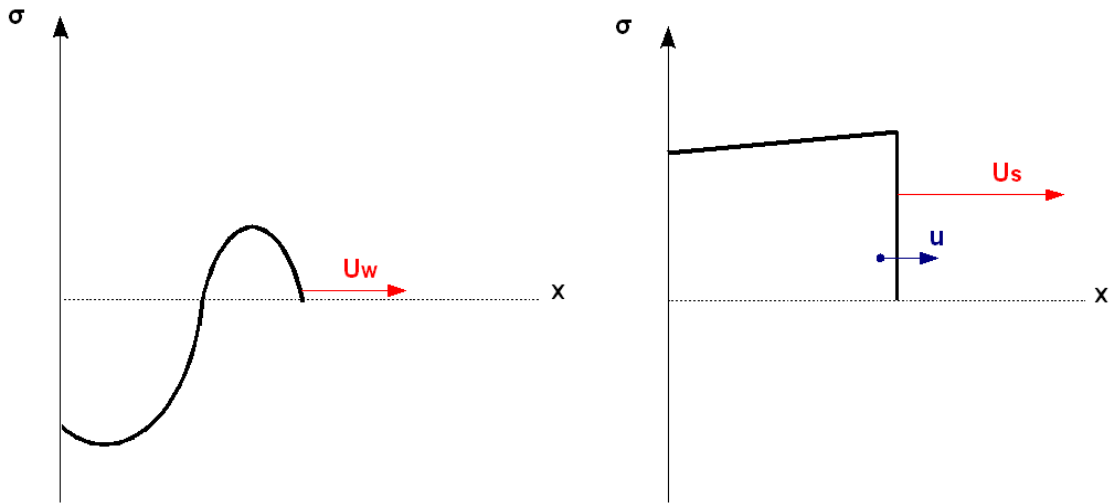
Figure 2.3: Mathematical functions representing a seismic wave (left panel) and a shock wave (right panel). σ is the stress and x the distance. The seismic wave moves with a velocity U_w and can be described by a continuous mathematical function (i.e. a sine function). The shock wave front moves with a velocity U_s greater than the particle velocity u. The slope of the shock wave front is equal to infinity, which corresponds mathematically to a discontinuity.
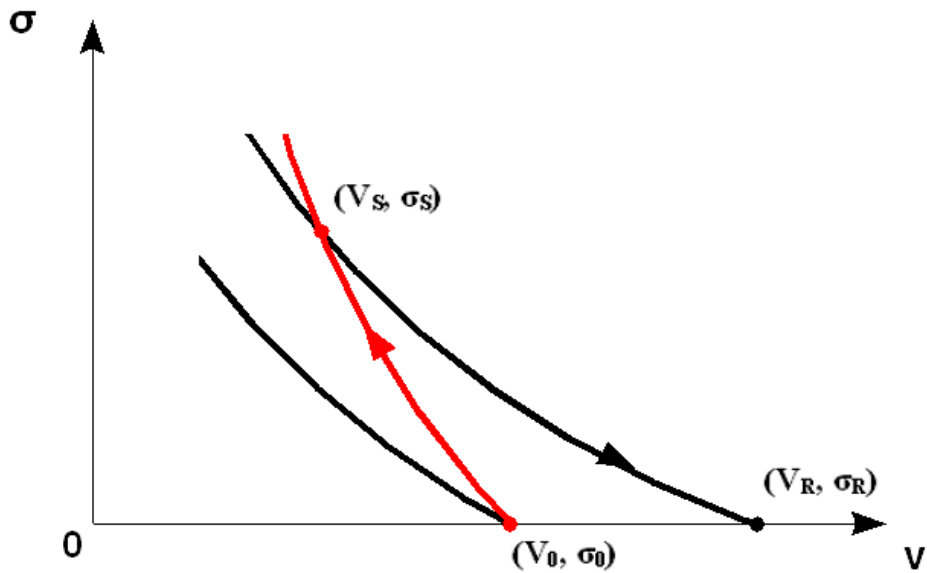
Figure 2.4: Stress and specific volume ($1/\rho$) diagram showing elastic behaviour curves (black) and a shock wave curve or Hugoniot (red). Any change one way or another along an elastic curve is reversible, while a change along the Hugoniot is not. For example a rock with initial conditions V_0 and σ_0 shaken by a shock wave will "jump" to (V_S, σ_S) just after the wave front has passed. Then the shock stress will be released following a different elastic curve than original to end up in (V_R, σ_R). Adapted from Isbell, 2005.
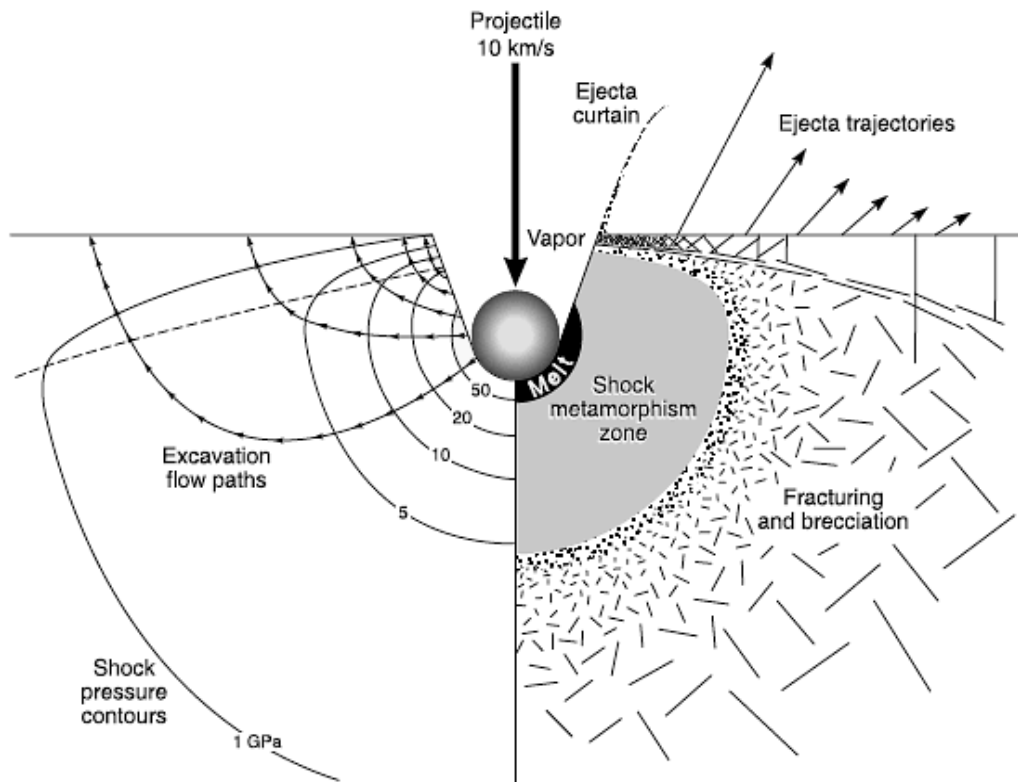
Figure 2.5: A simplified cross-section showing both maximum shock pressures and impact effects into the target rocks. Notice the rapid decrease of the shock wave stress. From French (1998).

Chapter 3

The Bosumtwi Impact Crater

3.1 Geology

The Bosumtwi crater is currently the largest young impact structure known on the surface of our planet. It is located in central Ghana, in Western Africa, only 6 degrees north of the equator. The crater diameter is 10.5 km, which puts it among the middle sized craters on Earth, and it is filled by a circular lake 8.5 km wide. The impact structure is 1.07 Ma old (Koeberl et al., 1998) while the target rocks consist of 2 Ga old metasediments and metavolcanic rocks. The Bosumtwi impact crater has been shown to be the source of the Ivory Coast tektite strewn field (Koeberl et al., 1997), that extends offshore several hundred kilometers west and south of the crater (Figure 3.1).

The crater was excavated in 2 Ga Proterozoic rocks from the Birimian supergroup (Figure 3.2). This supergroup consists of two units of the same age but very lithologicaly different (Leube et al. 1990). The first unit is composed of metamorphosed sedimentary rocks, mainly greywackes, quartzitic greywackes, phyllites, schists and shales. The second unit consists of with volcanic rocks weathered and metamorphised into the green schist facies (low grade metamorphism), and now exhibiting micashists, calcite-chlorite schists, and amphibolites. The crater footprint is mostly in the first described unit (metasediments), the second unit being present at the south-east edge of the lake and further in this direction.

Granitoid intrusions are also found in the Birimian. Their composition is mainly diorites and granodiorites (Wright et al. 1985). Some carbonates are found as well, whom, according to Appiah (1991), are the result of a pre-impact hydrothermal alteration of the Birimian rocks.

Impact ejecta material is exposed extensively around the crater (Jones et al, 1981). It consists mostly of monomict and polymict impact breccias. None of them display melt particles. Suevite outcrops are more scarce and found north and south-west of the crater (Chao 1968, Jones et al. 1981, Reimold et al. 1998). They exhibit target rock fragments representative of all the stages of shock metamorphism, along with impact melt particles (Karikari et al., 2007). After studying shallow drill cores from these areas, Boamah and Koeberl (2003) concluded there was no relationship between depth and clasts size in the suevite deposits, nor intensity of the impact metamorphism.

No ballen quartz were found within the crater (Ferrière et al., 2007) but some were found in the ejecta around the crater. PDFs observed in impactites and target rocks indicate an impact energy in these rocks of roughly 30 GPa. The presumed melt layer within the crater was not found (Ugalde et al., 2007b, Artemieva, 2007), only small melt particles were observed in the suevites. This constrains the pressure at the impact point to be between 45 and 60 GPa.

It was deduced from the geological information available and from modeling results by Artemieva (2007) that the impactor had a velocity greater than 20 km/s with an angle of incidence between 30 and 50 degrees. Although it depends on the velocity and the angle, the inferred diameter of the impactor was most probably of a few hundred metres.
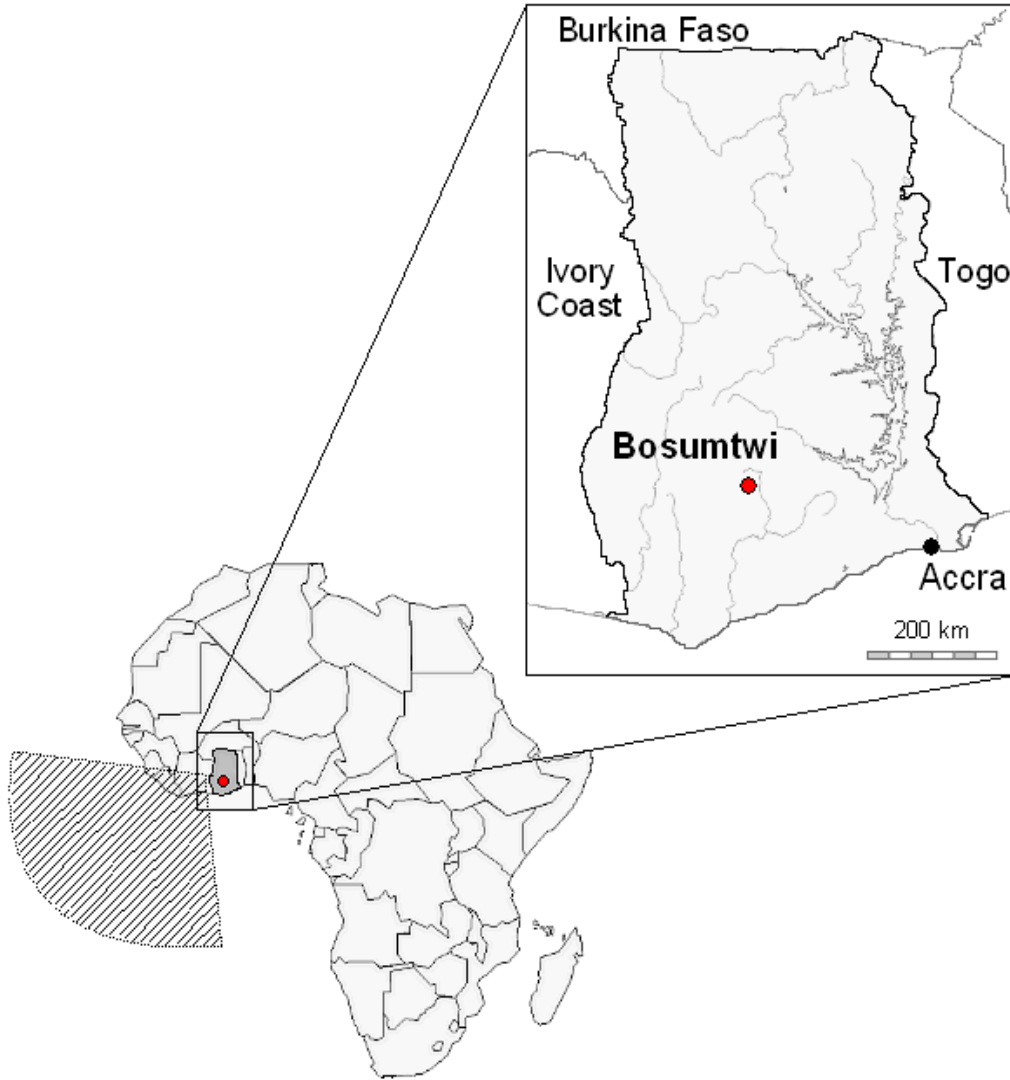
Figure 3.1: Location of Lake Bosumtwi within Ghana and Africa. The dashed area on the lower map indicates the tektite strewn field associated with the Bosumtwi impact crater. Original blank maps are from the Free Map Library (2009).
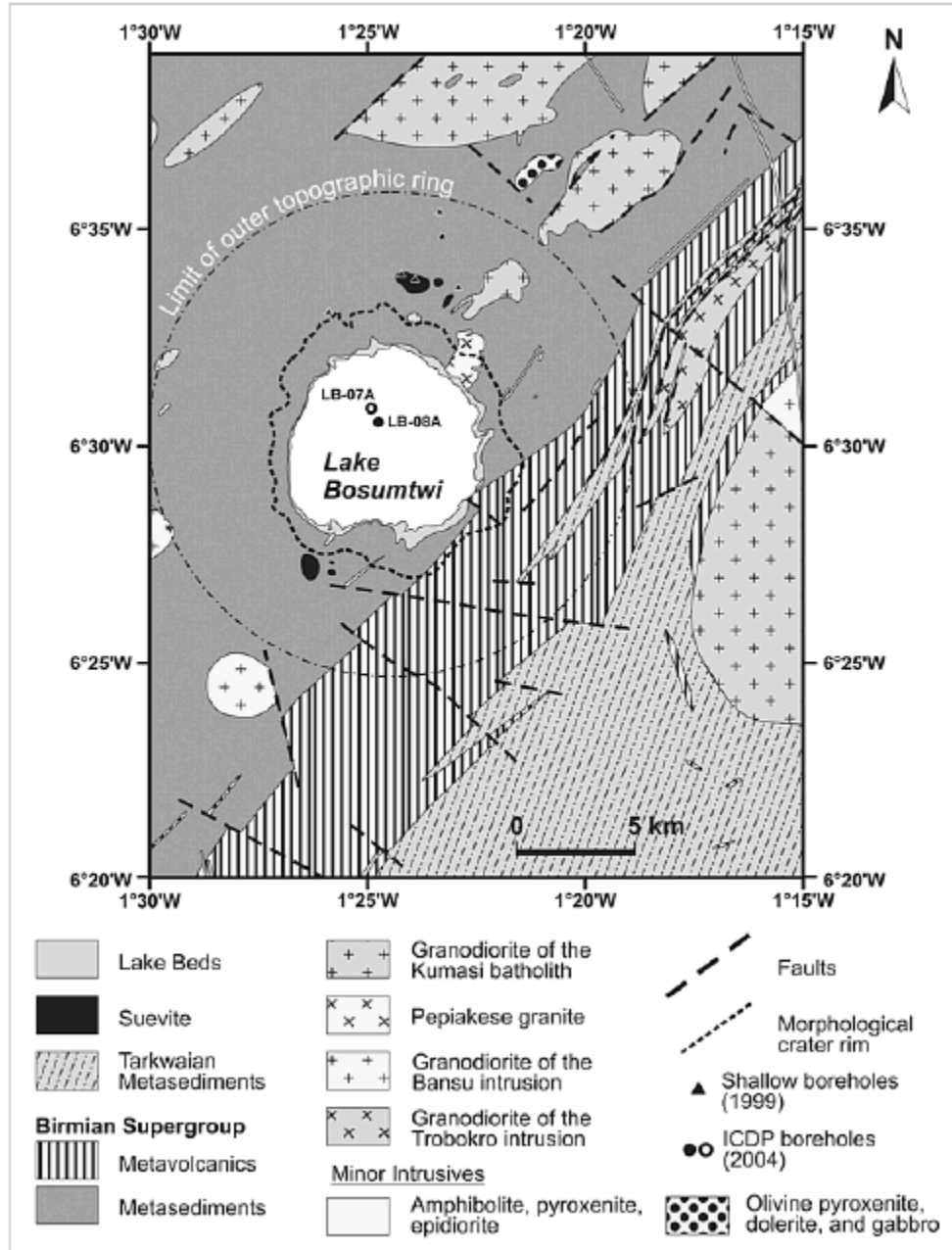
Figure 3.2: Simplified geologic map of the Bosumtwi crater area. From Koeberl and Reimold (2005).

3.2 Geophysical data

3.2.1 Topometry

Jones et al. (1981) were the first to set up a detailed topographic map of the crater area. They noticed that the watershed follows the rim of the crater except in the south, where the influence of the Obuom Mountain Range shifts the watershed further away from the lake. As shown on Figure 3.3, the crater rim is pronounced and rises between 250 m and 300 m above the surface of the lake, which has a maximum depth of 80 m. An outer ring of about 20 km in diameter can also be seen.

3.2.2 Gravimetry

In 1999, a gravity measurement campaign was conducted on land around the lake, and in 2001 additional measurements were performed on the lake (Danuor and Menyeh, 2007). After compilation and correction of all the data, Ugalde et al. (2007a) obtained the final Bouguer gravity anomaly (Figure 3.4). As expected the map shows a strong negative anomaly of about 15 mGal centered on the lake. This mass deficiency can be explained by the target rocks being fractured and by the low density sedimentary and breccia fill of the crater.

3.2.3 Magnetism

In 1997 a high resolution aeromagnetic survey was conducted by the Geological Survey of Finland, the University of Vienna, and the Ghana Geological Survey Department (Pesonen et al., 1998). The residual magnetic field (after regional field correction) shows a negative anomaly in the central north part of the lake (Figure 3.5), associated with positive anomalies on the northern and southern parts of the lake. This magnetic signature is expected at this latitude. Weaker negative anomalies just south-east and south-west of the previous one,

circle the center of the crater, and possibly indicate the presence of a central uplift. Modeling by Plado et al. (2000) predicted a magnetized melt-rich lens body within the crater, into the impact breccias level.

3.2.4 Seismic studies

An extensive surface seismic survey was run in 1999. Refraction seismic was acquired on two lines across the lake and its rim. Reflection seismic was acquired along several lines forming a grid over the lake. Figure 3.6 shows the velocity model obtained from the refraction seismic by Karp et al. (2002). We can see a dramatic change in velocity between the lake sediments and the hardrock basement, as well as a strong increase of the velocity with depth in the hardrock. A central uplift is also seen in the middle of the model. Scholz et al. (2002) imaged this central uplift in detail. Figure 3.7 shows an interpreted reflection seismic line running across the lake. Numerous reflectors are seen in the sediment fill of the lake. Then a strong reflector marks the top of the brecciated layer. Below this reflector the hard rocks are seismically transparent (i.e. no coherent events are seen in the image). The central uplift, buried beneath lake sediments, exhibits several faults. Some of them are continuing upwards into the sediments, which indicate post-impact tectonic activity. This may be due to a differential compaction of the impact brecciated rocks (which are expected to have a very high porosity).
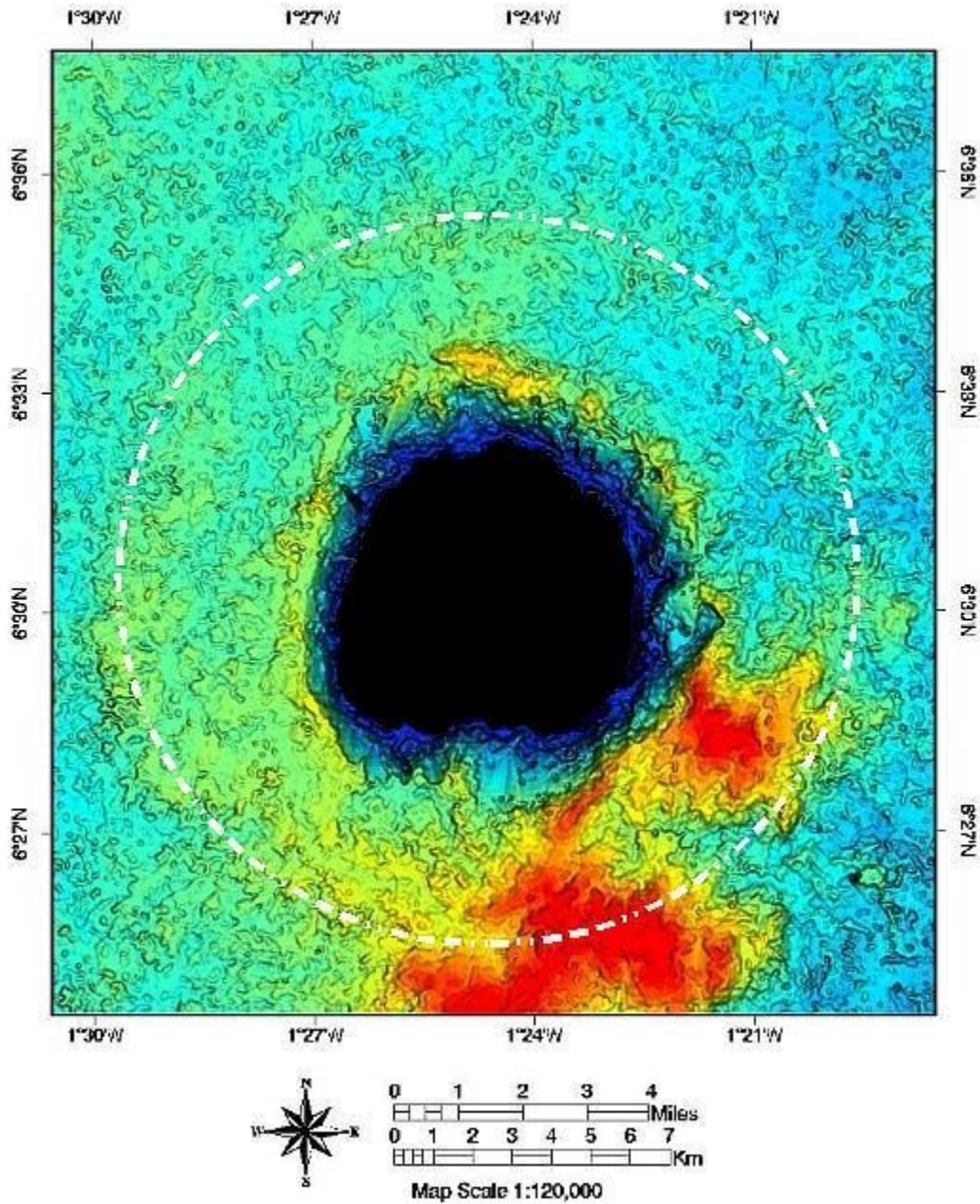
Figure 3.3: Digital Elevation Model of the Bosumtwi crater area. Hot colors are higher elevations, cold colors lower elevations. The lake surface was not modeled and appears in black. The dashed white line indicates the faint outer ring. Modified after Earth Impact Database (2008).
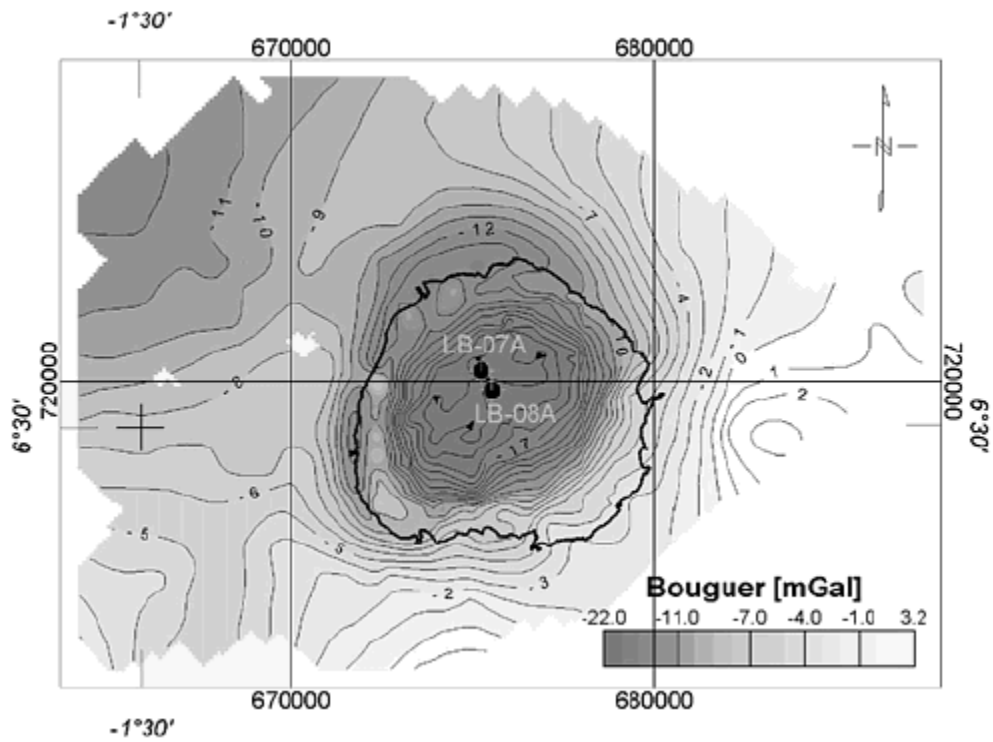
Figure 3.4: Bouguer gravity anomaly map of Lake Bosumtwi. Contour interval is 1mGal. Black triangles mark the maximum negative of the anomaly. From Ugalde et al. (2007a).
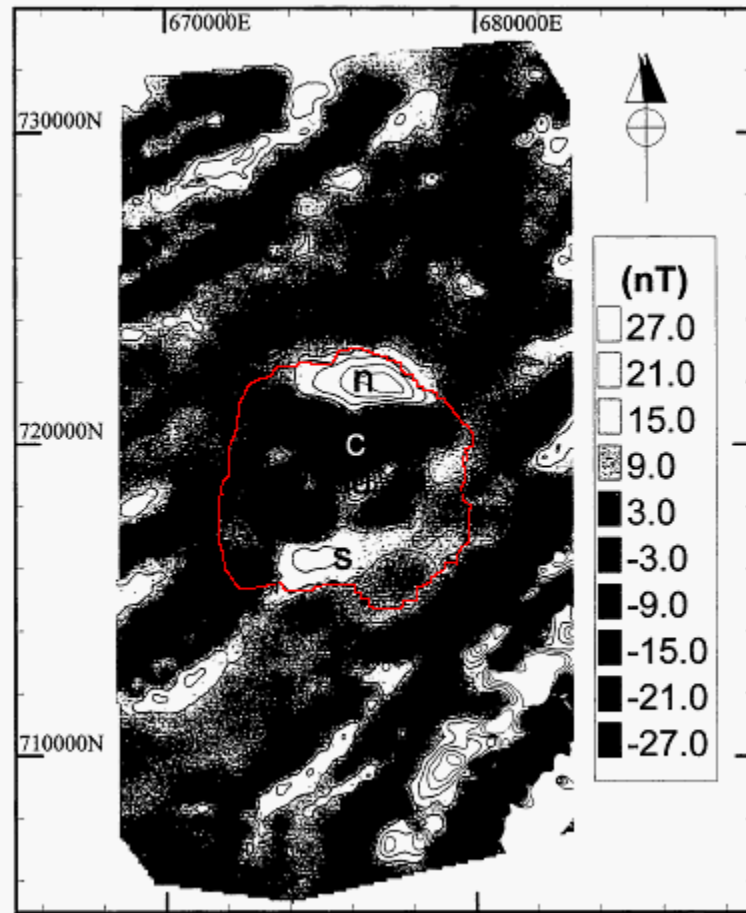
Figure 3.5: Residual magnetic field map of the Lake Bosumtwi area. The red line marks the lake shoreline, *n* and *s* indicates the North and South positive anomalies, *c* central negative anomaly. Contour interval is 6 nT. Adapted from Plado et al. (2000).
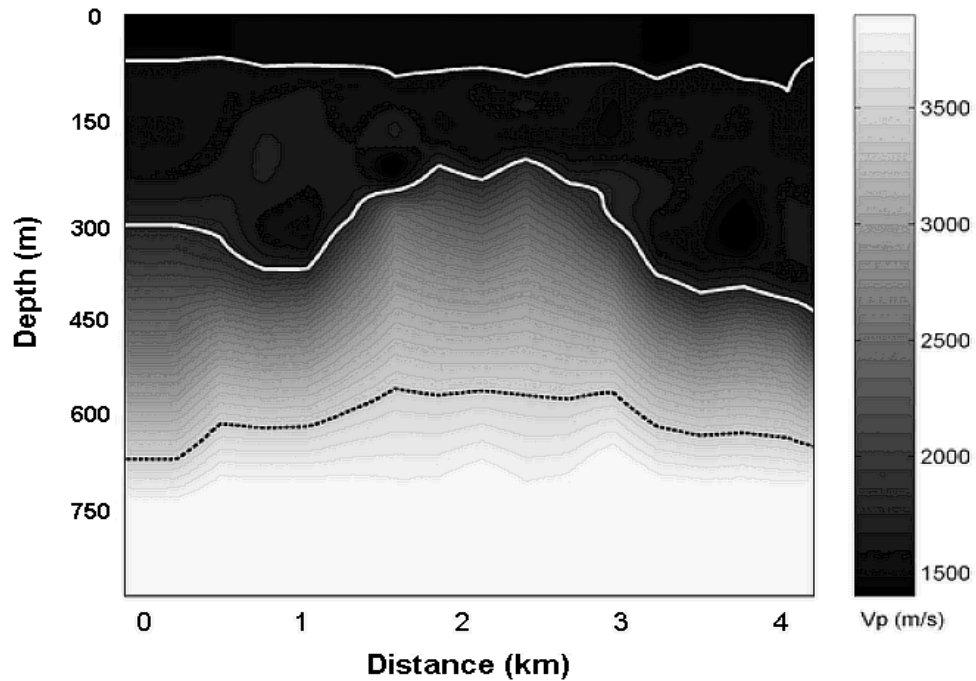
Figure 3.6: Velocity model of the crater structure obtained from refraction seismic. Contours starting from the surface represent 1480 m/s, 1800 m/s and 3500 m/s. From Karp et al. (2002).
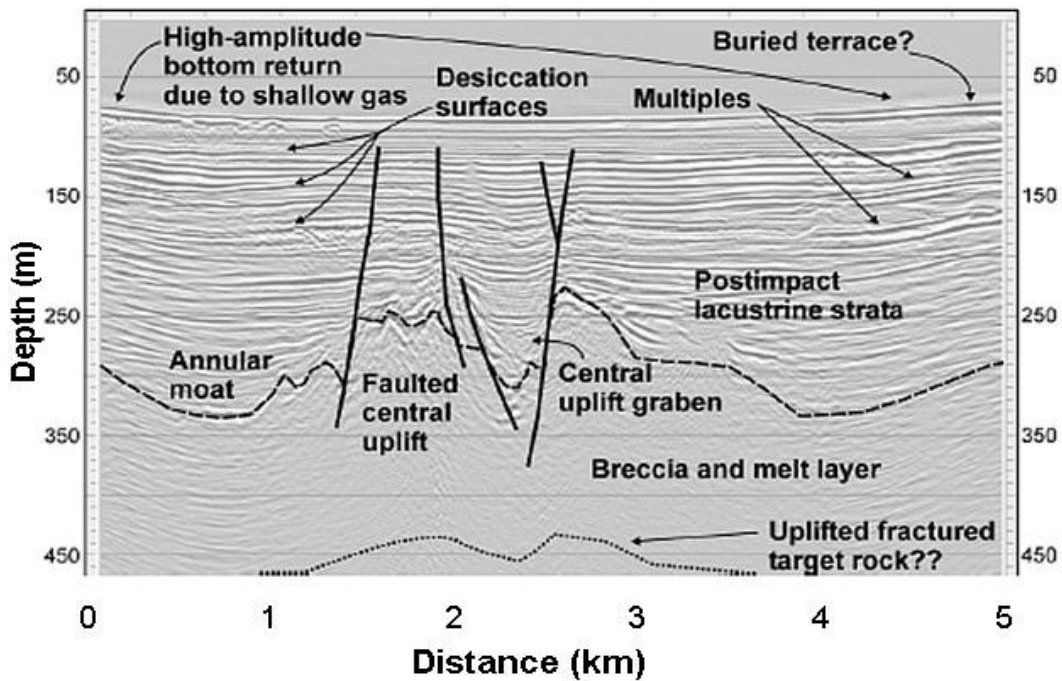
Figure 3.7: Interpreted reflection seismic line across Lake Bosumtwi. From Scholz et al. (2002).

Chapter 4

Drilling Project

4.1 Overview of ICDP program

The International Continental Scientific Drilling Program is an international project associating universities from over the world with the goal of improving and widening our knowledge of the continental crust, including its composition, structure and evolution. Forty eight projects are running or have been completed so far. Objects of interest range from ore bearing crystalline rocks like in Outokumpu, Finland, or Sudbury, Canada, to active tectonic zones such as the North Anatolian Fault in Turkey, or the Dead Sea basin in Israel. Impact cratering being an essential process in the evolution of the crust of telluric planets, impact structures are privileged targets as well. Projects are carried out in giant craters like Chixculub in Mexico, submarine craters like Mjølnir in Norway, or in our case young preserved craters like Lake Bosumtwi, Ghana.

The Bosumtwi Drilling Project was started in 2000, and the field operations ended in the fall of 2004. The crater structure being buried below a lake and sediments, drilling was the only way to obtain further geological and geophysical information than already achieved.

First it is an extraordinary opportunity for paleoclimatic and environmental studies. Located in the intertropical zone, the post-impact sediments accumulated in its lake offer a one million year record for climate changes in a region of the world that has very little data in this domain.

Then, as a young crater, Bosumtwi is well preserved and provides a rare opportunity to examine the consequences of impact at many scales. It is a medium size crater, just above the transition size between small simple craters and bigger complex craters. Hence the structure and fill of the crater are of high scientific interest. All this can be investigated through correlating geochemical and geological data with previous and new geophysical observations, as well as petrophysical measurements on the drill cores. The core samples extracted from the hardrock basement of the crater are a unique chance for studying in detail impact damaged rocks.

Six shallow drill holes were cored into the lake sediments for paleoclimatic studies (Koeberl et al. 2007). Some of them go as deep as 250 m. They are regularly spaced on a line going from the center of the crater to the shore of the lake.

For our concern two deep boreholes reaching the hardrock basement were drilled into the crater. LB-08A in the central uplift down to 451 m below the lake surface, and LB-07A in the circular basin around it, down to 545 m (Figure 4.1). The upper part of the holes drilled through the water gorged sediments had to be cased to prevent it from collapsing. The lower part of the holes, into hard rocks, is open. Core samples were collected all along the holes and geophysical loggings along with televiewer data were acquired during the drilling operations, both through the casing and in the open hole section. A VSP (Vertical Seismic Profile) survey was also performed thereafter in the two boreholes, with two main goals: to further examine the transparent or no-reflection zone seen on the reflection seismic (Figure 3.7); and to get detailed seismic velocity profiles along the holes.

4.2 Physical properties framework

4.2.1 Lithostratigraphy

The stratigraphic column of borehole LB-07A exhibits lake sediments over 250 m. The hard rock basement is reached at a depth of 333 m. The open hole

section shows a well stratified basement with alternating lithologies from 333 to 545 m (Figure 4.2). First is met a consistent layer of polymict breccias (30 m thick). Then breccias alternate with suevites until 412 m deep, where the lithology changes to monomict breccias. This sequence was expected as the first two lithologies represent the ejecta and slumped rocks deposited after the impact event, while the last lithology is basically the damaged and recemented target rock (metapelites in this case). The lower part of the hole displays the autochtonous shales and phyllites, with a few suevite dykes and meta-greywacke levels.

LB-08A was drilled through a thinner sediment layer (160 m). The open hole section, from 236 to 451 m, does not show any clear organization, except from the polymict breccia layer at the very top (25 m thick). These are the only impactites present in this borehole. The rest and most part of the borehole displays mainly greywackes often alternating with phyllite and shale layers and crossed by numerous suevite dykes. The bedrock is met much higher on this borehole than on the previous one, and is much more disturbed. This is indicative of the formation of the central uplift by uprising of the bedrock.

4.2.2 Wireline loggings

A range of in situ, continuous, physical measurements were performed in the boreholes: gamma ray spectrometry, caliper (borehole diameter), magnetic susceptibility, and electrical resistivity (Figure 4.3). In addition acoustic televiewer data and P-wave sonics were acquired. These last measurements are detailed in the latter sections. Direct in-situ porosity measurements are impossible to perform, but porosities can be inferred from the previous measurements.

A three-arm caliper measured the diameter of the hole in two perpendicular directions. On average the borehole diameter is 10.0 cm in the greywackes and phyllites, and 10.4 cm in the breccias (Hunze and Wonik, 2007). This may be due

to a lower compaction of the breccias, or may indicate a more damaged state.

Density and magnetic measurements in both boreholes show low-amplitude contrasts between the different lithologies (Morris et al. 2007). Hence no discrimination can be made between impactites and target rocks.

Resistivity was measured using a dual current tool. This technique allows for corrections due to possible fluid invasion into the drilled rock. Porosities were then inferred from the measured resistivity values. They are in good agreement with laboratory measurements on drill cores from the previous 2004 survey (Ugalde et al., 2007). The very high porosity values obtained for the impactites (up to 30%) may have important mechanical implications for the stability of these rocks.

The main issue with these kinds of measurements is that in addition to the impact event, they are influenced by numerous parameters such as lithology, borehole conditions, drilling perturbations, or pre-impact structures. All this makes it almost impossible to discriminate the impact induced properties of the rocks without integrating the loggings with further geophysical data.

4.2.3 Televiewer

An example of acoustic televiewer recording is shown on Figure 4.4. The data acquired in the open hole section of LB-08A shows a very high density of planar structures (more than three per metre), most of which are open fractures. Koeberl et al (2007) analyzed 50 m of this open hole section. For several reasons it was not possible to orient the numerous drill cores and extend this study to a greater depth. Results on Figure 3.5 show a random distribution of dip directions for the planar structures. Another study by Hunze and Wonik (2007) on the whole open section of LB-08A shows two main dip directions for fractures, to the south-east and to the south-west (Figure 4.5). Obtained dip angles are quite steep, ranging from 50 to 70 degrees.

We see from these two contradictory results that it is impossible to extend

local characteristics of the rock structures to a global trend. Possible explanations are the complex motions of the damaged target rocks induced by the formation of the crater, and the complicated lithostratigraphy of the rocks within the crater. Hunze and Wonik (2007) concluded that it is not possible to tell whether the structures observed with the televiewer represent consequences of the impact event or not.

4.2.4 Sonic

Sonic velocities of the P wave were measured in the borehole every 10 cm. The frequency used is around 20 kHz. Figure 4.6 shows the profile obtained in hole LB-08A. Once again, there is no obvious correlation between the lithology and the measurements.

As one can see, this is a very high resolution velocity profile. In order to get the general trends and compare it later with the seismic, we smoothed this profile using various averages. First, we calculated a standard arithmetic mean:

$$V_A(z) = \frac{\sum\limits_{i=1}^{N} V(z_i)}{N}$$

where V_A is the arithmetic averaged velocity at a depth z
$V(z_i)$ is the sonic velocity for the sample i
N is the number of samples

A Backus average, representing a low frequency approximation, was also calculated:

$$V_B(z) = \left(\frac{\sum\limits_{i=1}^{N} V^{-2}(z_i)}{N} \right)^{-1/2}$$

And finally, a high frequency harmonic average was computed:

$$V_w(z) = \frac{N}{\displaystyle\sum_{i=1}^{N} V^{-1}(z_i)}$$

We can compare the three curves obtained in Figure 4.6. The Backus and harmonic averages represent the low and high frequency limits, respectively (Rio et al., 1968). The arithmetic average does not physically represent anything, but is circumscribed by the other two curves. This given, the three curves are very close to each other, and show the same variations. In a general way, velocity is increasing with depth, from 2500 m/s at 240 m deep, to 3500 m/s at 420 m deep. This represents an increase of 40% over 180 m. On the last 30 m, velocity quickly drops to 2700 m/s before going up again.

These results are compared with those from the VSP survey in section 5.3.
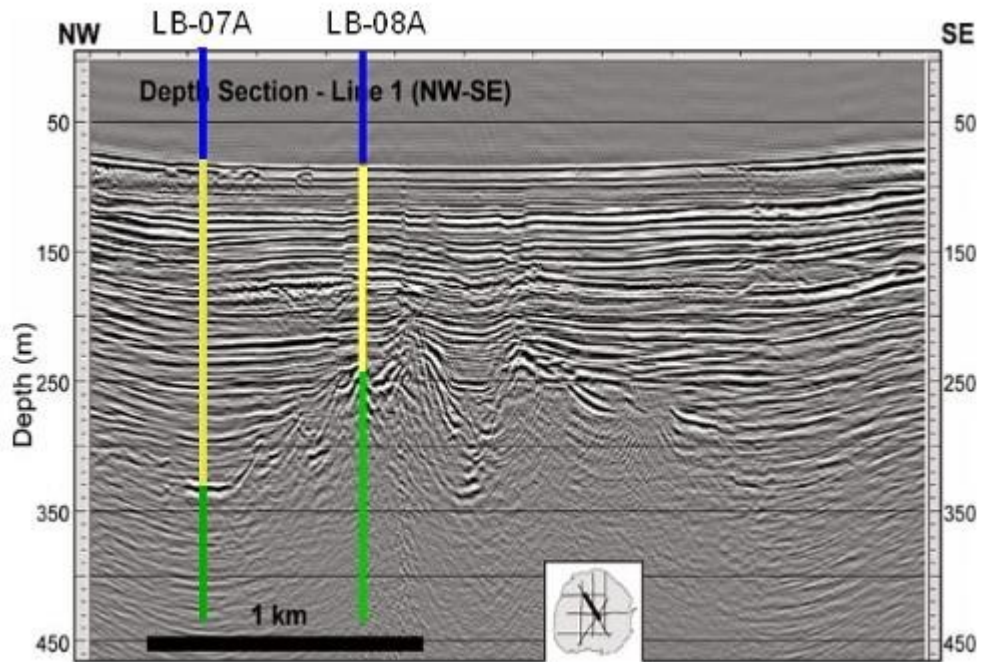
Figure 4.1: Location of the two deep boreholes on a reflection seismic transect. Blue represents the steel casing in the water column, yellow represents the PQ casing in the weak sediments, green represents the open hole section in the hard rock. Adapted from Scholz et al. (2002).
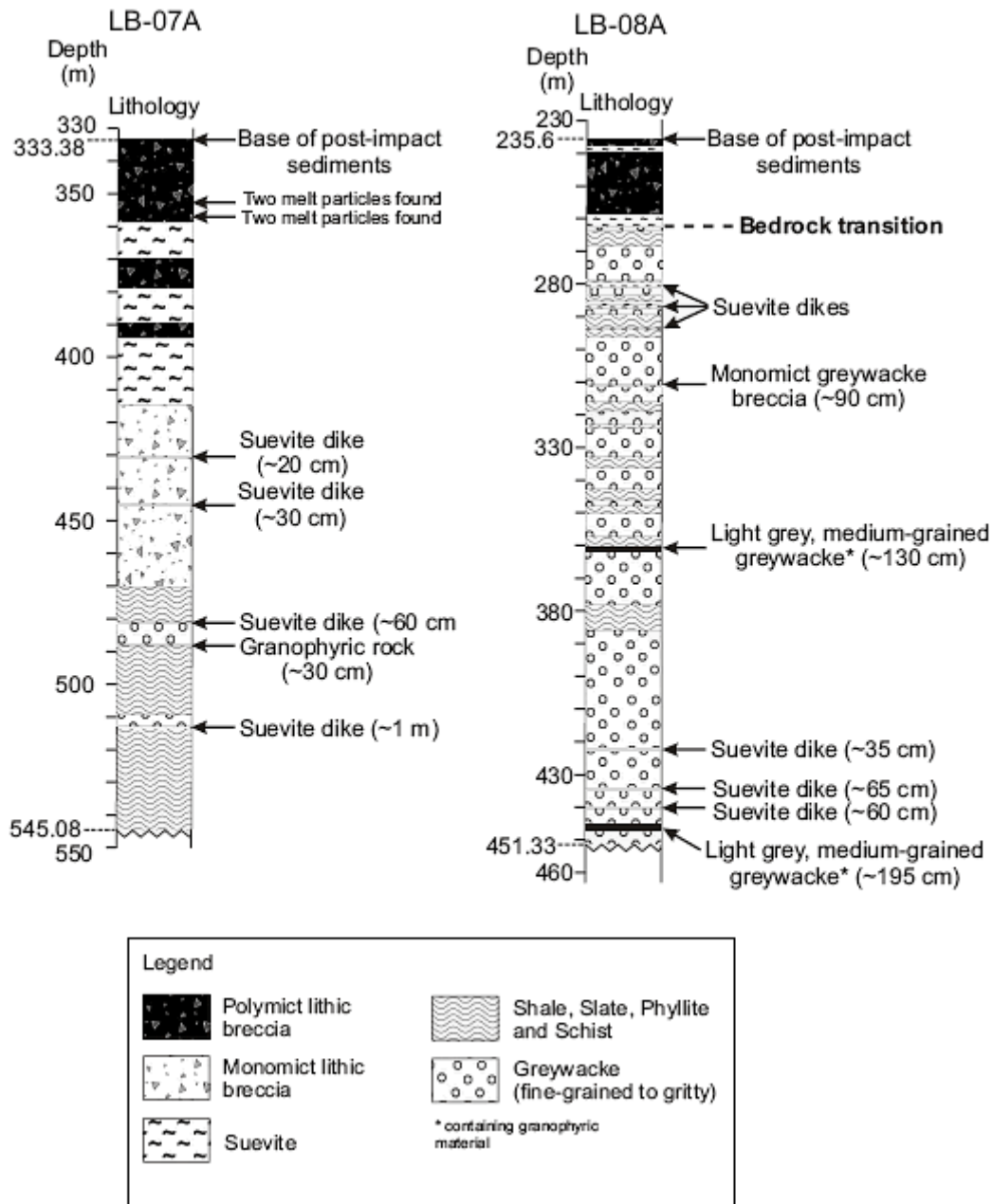
Figure 4.2: Simplified lithostratigraphy for the deep boreholes LB-07A and LB-08A.
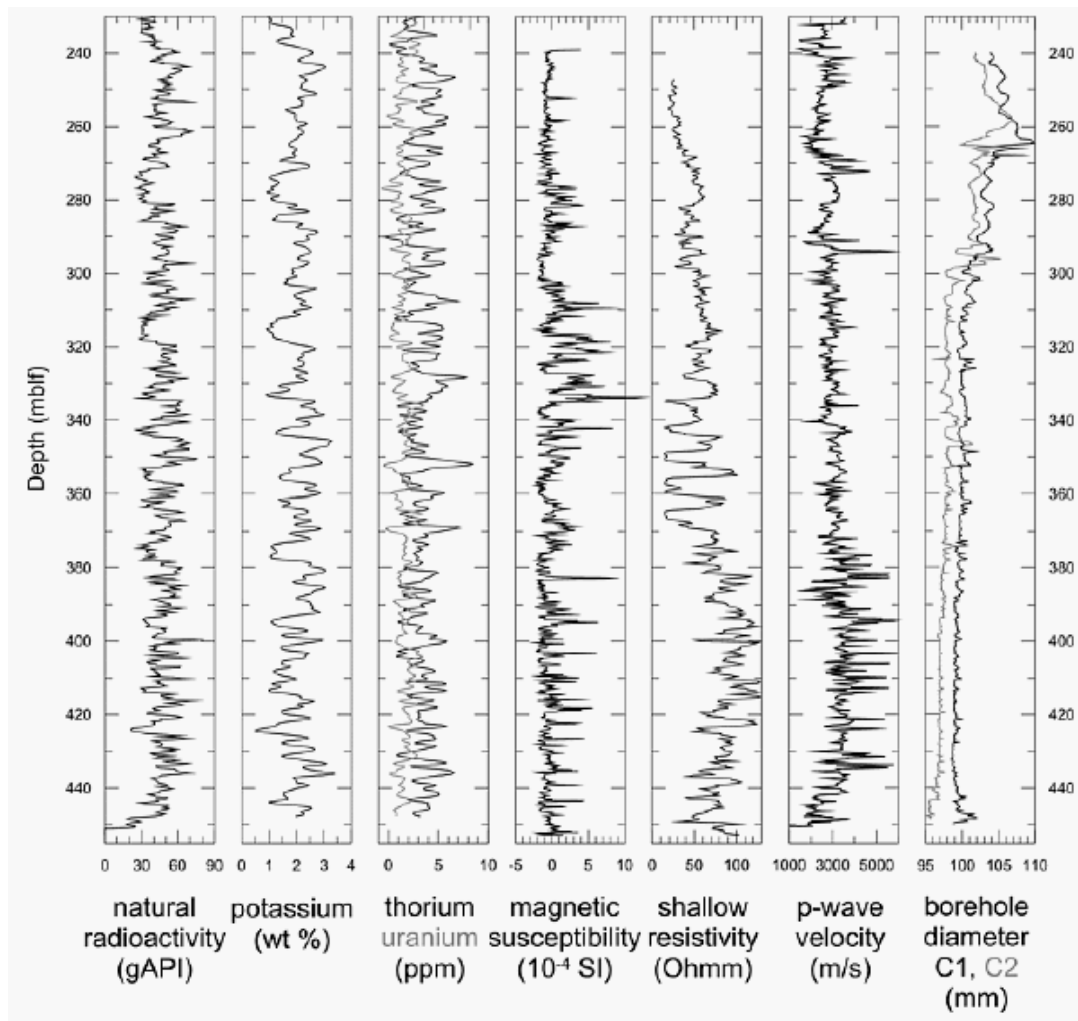
Figure 4.3: Wireline loggings in the open hole section of borehole LB-08A. From Hunze and Wonik, (2007).
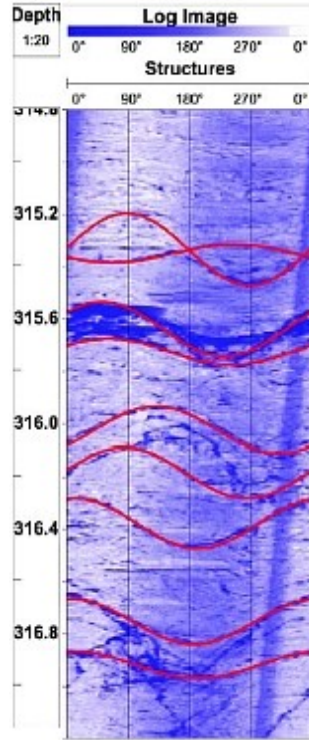
Figure 4.4: Example of televiewer image from borehole LB-08A. Nine planar features (in red) are counted over two metres. Adapted from Koeberl et al. (2007).
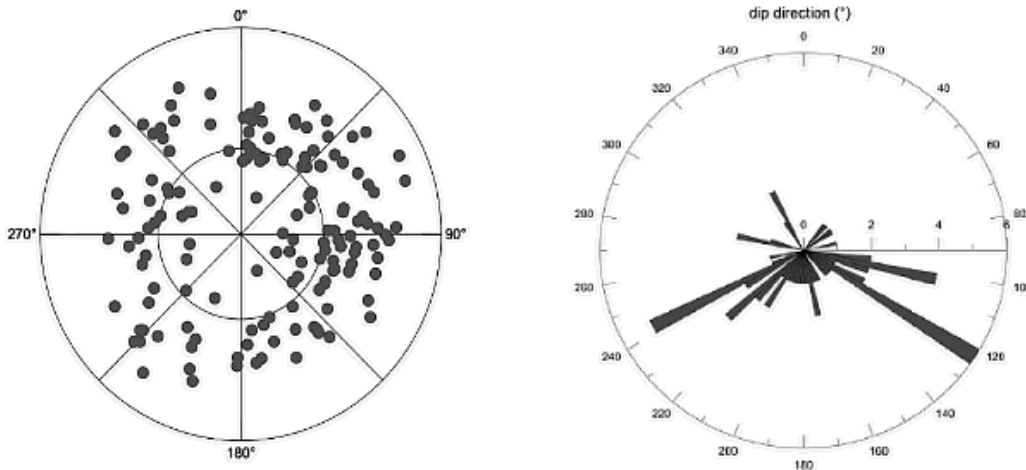
Figure 4.5: Dip directions from televiewer data for borehole LB-08A. Left panel is an analysis by Koeberl et al. (2007), showing dip directions of all the observed planar features over 50 m of the open hole section (from 290 to 343 m). Right panel is an analysis by Hunze and Wonik (2007) showing dip directions for identified fractures over the open hole section (from 238 m to 455 m).
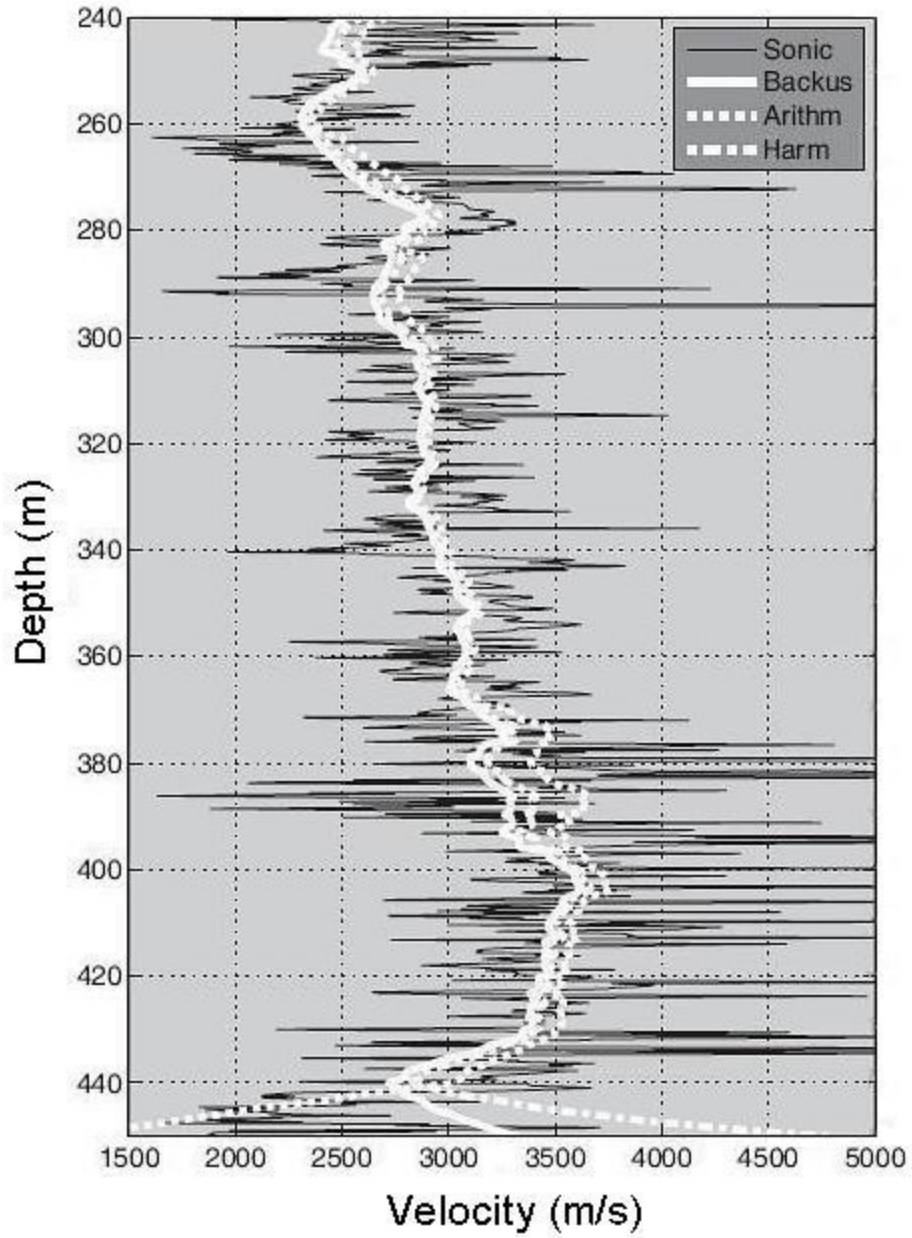
Figure 4.6: Sonic averages for the hardrock part of borehole LB-08A. Sonic: raw field data, Backus: Backus average (low frequency approximation), Arithm: arithmetic average, Harm: harmonic average (high frequency approximation).

Chapter 5

Seismic Survey

5.1 Methods

Zero offset vertical seismic profiles were acquired in both LB-07A and LB-08A. The seismic source was a marine air gun (40 cubic inches displacement) placed at a depth of 10 m from the surface and operated from the shooting boat 'Kalindi'. A vertical component seismometer equipped with a well-locking system was placed into the hole and wired trough the portable GFZ system to a Geode® recording system. A few fiducial receivers of different frequencies (14 and 40 Hz) were placed on the lake surface, next to the boat, to help account for the possibility of triggering errors. Seismic data were recorded with a sampling period of 125 μs, and a pre-trigger time of 220 ms followed by a listening time of 1828 ms (total recording time was 2.048 s). For LB-08A a seismic trace was acquired every meter, from 50 m (near the lake bottom) to 453 m deep, over two days in October 2004. We will focus on these data in this study. Unfortunately the data acquired in LB-07A were of too poor quality to obtain useful information.

5.2 Vertical Seismic Profile

5.2.1 Processing

The raw VSP data, shown on Figure 5.1, display many features that are not easily interpreted. First we notice low-frequency reverberations (with periods of

approximately 50 ms) all along the profile. This is the so called bubble effect, always present on marine seismic data that employs air gun. Then we can see another kind of ringing noise with a shorter period (around 12 ms). This noise has a very strong amplitude just above the bottom of the casing and, though hard to identify, is probably related to tube waves (waves propagating in the steel casing) or movements of the casing with respect to the weak sediments. Note this noise is absent in the lower part of the profile, in the open hole section. Also in the upper part, some upgoing tube waves are visible just after the first break, at a depth of 150 m and above.

By applying a band-pass filter the low frequency (around 20 Hz) bubble effect was removed. The higher frequency noise cannot be removed with this technique without affecting the signal. Hence we applied a predictive deconvolution to the data, which removed most of this noise. The upgoing tube waves in the upper part of the profile were also removed by this processing. The final processed profile is shown on Figure 5.2. The noise that is left just above 239 m before the second arrival is probably a tube wave, given its velocity and its arrival time.

5.2.2 Seismic velocities

Several arrivals are clearly visible on the processed Vertical Seismic Profile (VSP). Figure 5.3 shows the interpreted profile. The first arrival in the upper part (green line) has a velocity of 5200 m/s, which is the velocity of the P-wave in steel. This wave stops at the bottom of the casing. The second arrival (light blue) in the casing part of the profile is also a P-wave, propagating at 1520 m/s in the water gorged sediments. Continuous with this arrival, below the casing, is a strong P-wave propagating through the hard rock (dark blue). A secondary arrival is seen (yellow), from 239 m until 350 m. Originating at the casing bottom, this is probably a shear wave generated by decoupling between the casing and the weak sediments. these two waves propagating in the hard rock do not have a constant velocity. Their arrival times were picked in order to determine their velocity as a function of depth. Velocity profiles are presented in Figure 5.4. P-wave velocity

34

increases from 2500 m/s to 3250 m/s between 239 m and 451 m deep, and S-wave velocity increases from 1000 m/s to 1100 m/s between 239 m and 350 m deep. The P-wave velocity impressively increases by 30% over 210 m.

Both P and S velocities are lower than expected for low-grade metamorphosed sediments (Cholach, 2005). However, the Vp/Vs ratio, increasing from 2.5 to 2.75, is in the range of expectation for such rocks.

5.2.3 Wavefield separation

The last step in processing the VSP data was to separate the upgoing-wavefield and the downgoing-wavefield. As we were looking for reflections in the hard rock part of the crater, we focused on the open hole section of the profile (below 239m). To obtain the upgoing waves, we used two different techniques. One is the median filter method as described by Hardage (1983), the other one is a f-k filter method (Schmitt et al, 2007). Both methods yield a empty upgoing wavefield (Figure 5.5). This is in accordance with the results of Karp et al (2002), showing a seismically transparent bedrock on reflection data.
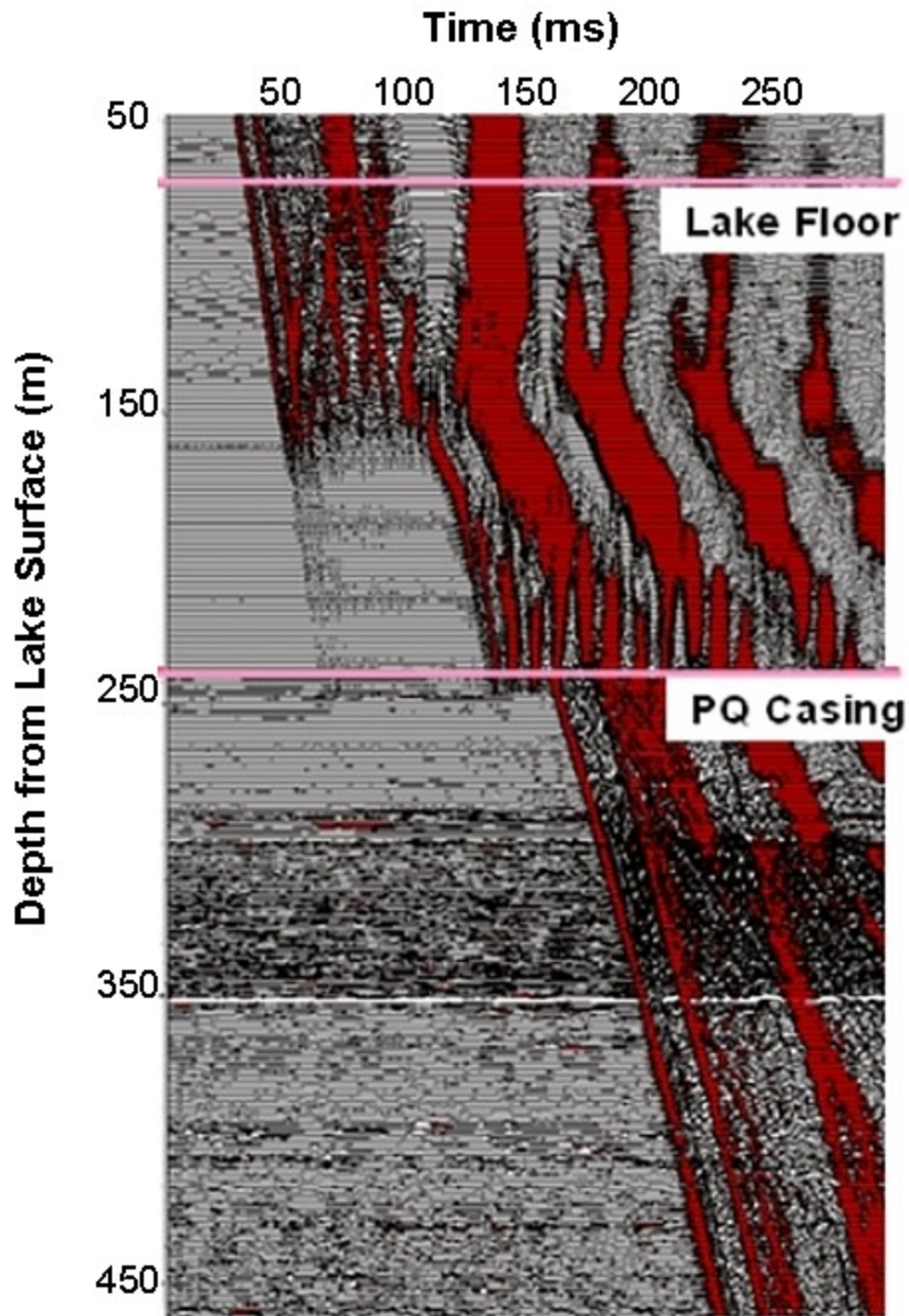
Figure 5.1: Raw Vertical Seismic Profile from borehole LB-08A. Pink lines represent the bottom of the lake (top of the sediments) and the bottom of the casing (top of hard rock).
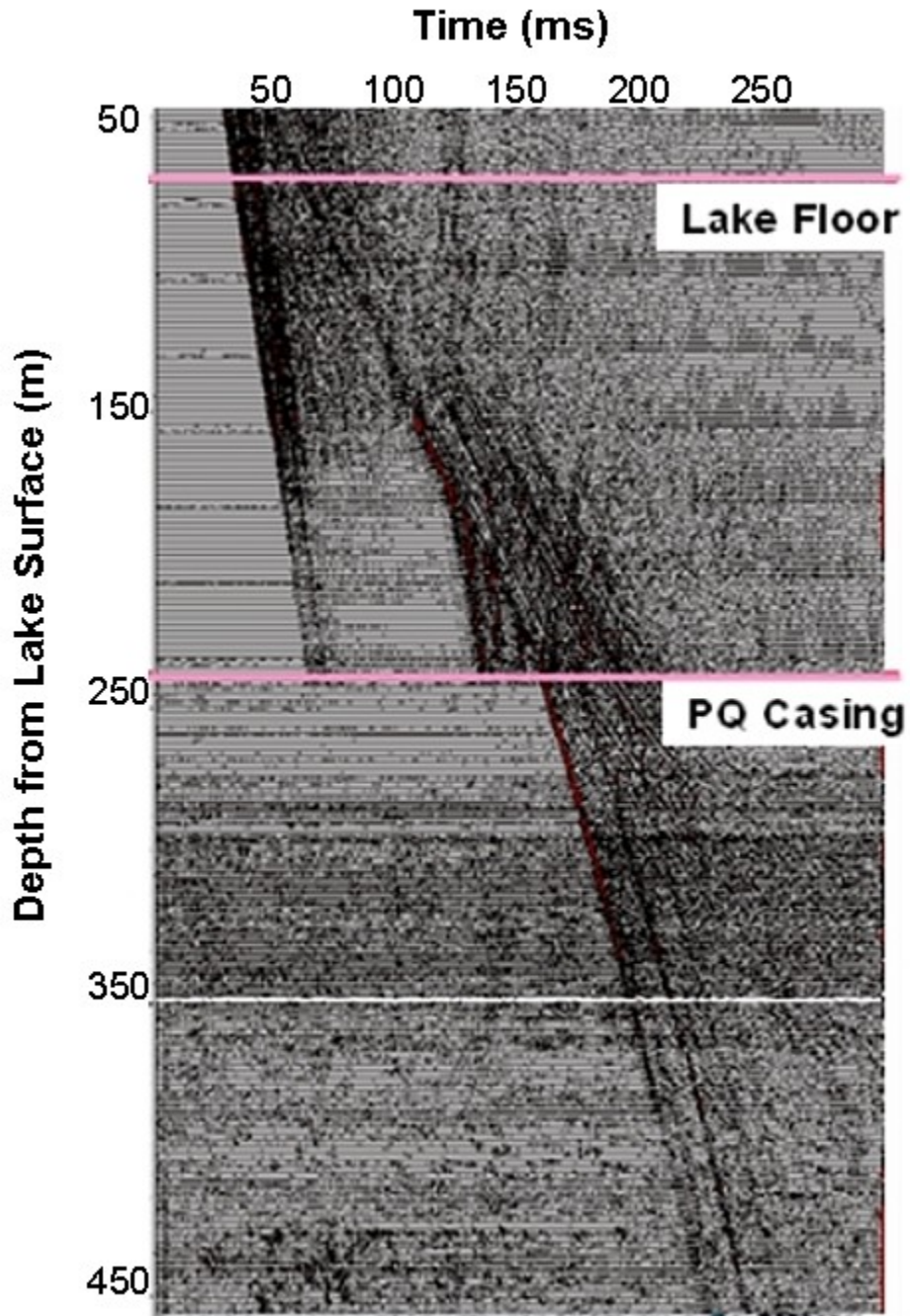
Figure 5.2: Final processed VSP from borehole LB-08A. Though most of the noise was removed, note the residual tube wave in the lower part of the cased section. Pink lines represent the bottom of the lake (top of the sediments) and the bottom of the casing (top of hard rock).
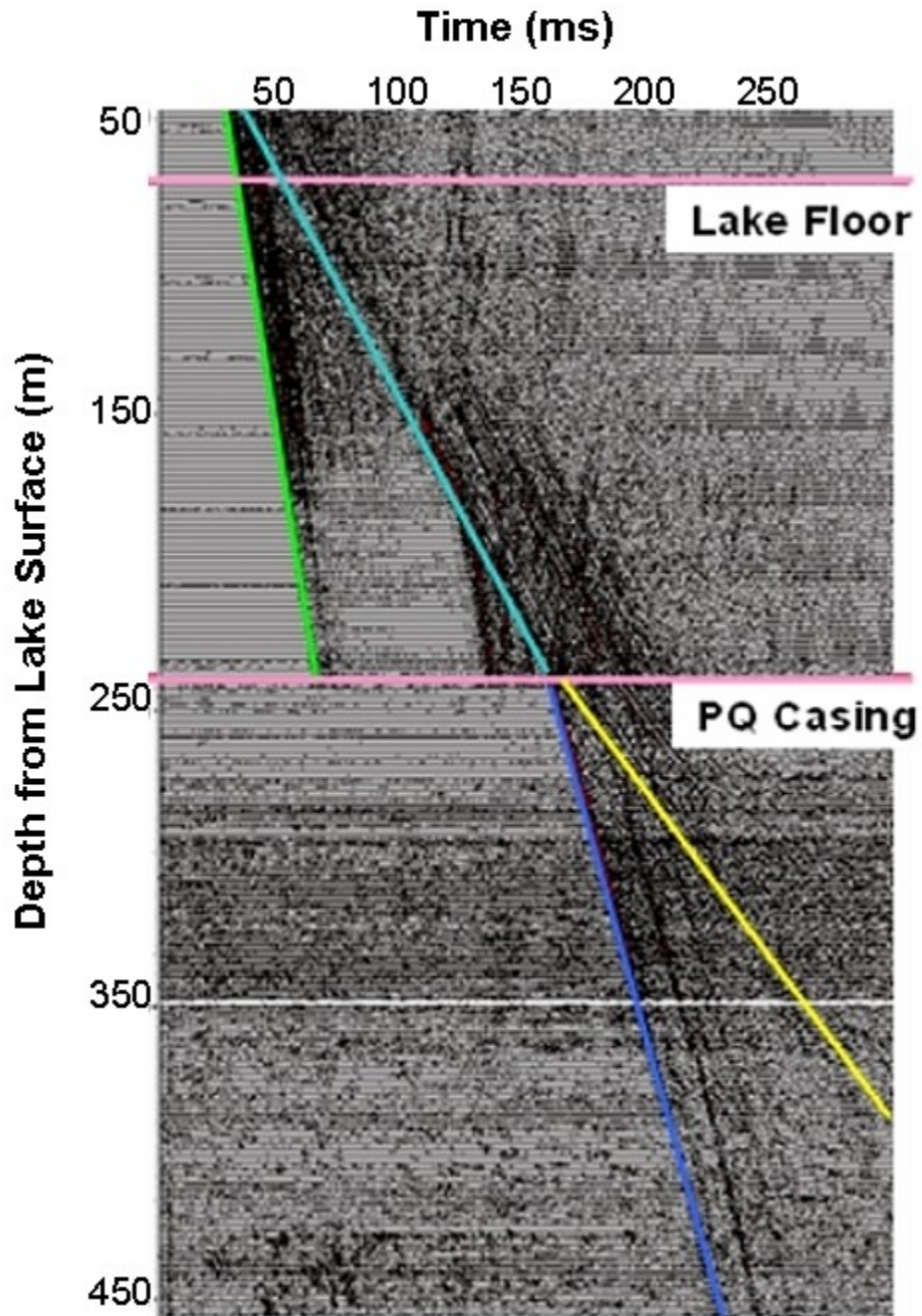
Figure 5.3: Interpreted VSP from borehole LB-08A. Green: P wave propagating in the steel casing. Light blue: P wave in the sediments. Dark blue: P wave in the hard rock. Yellow: secondary wave in the hard rock.
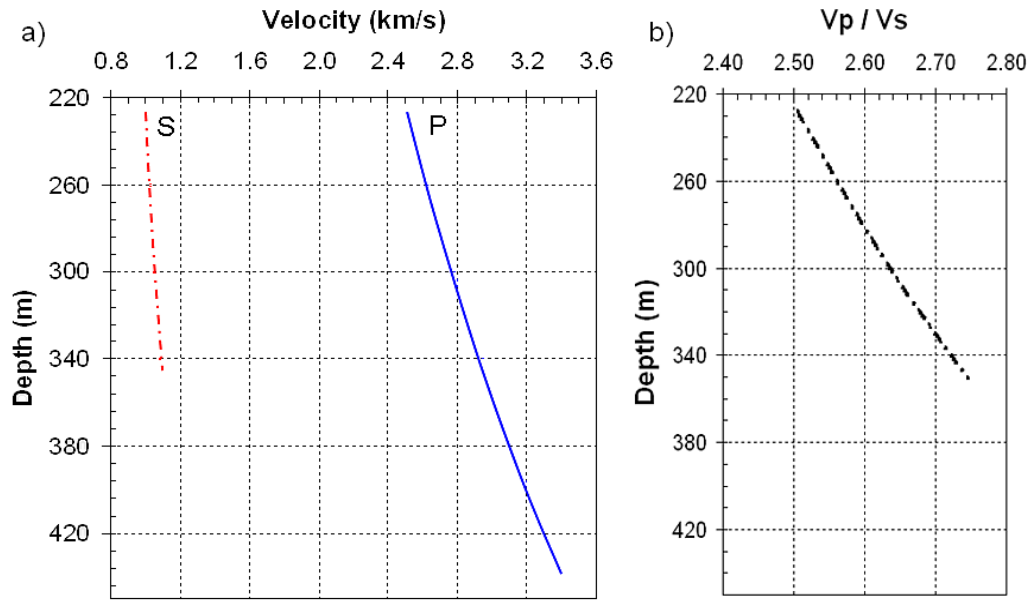
Figure 5.4: a) P and S wave velocities in the hard rock section. b) P and S wave velocity ratio.
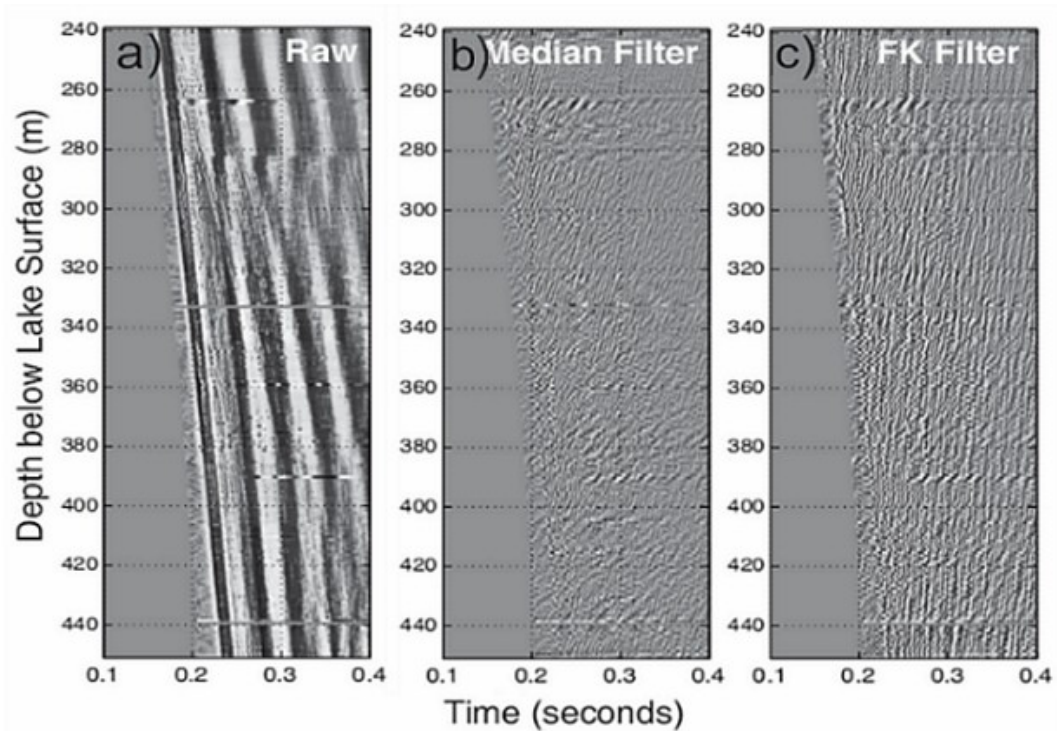
Figure 5.5: Upgoing wavefield obtained with two different methods. a) Raw data (full wavefield) b) Upgoing wavefield using a median filter c) Upgoing wavefield using a f-k filter.

5.3 Comparison of VSP with sonic

We can now compare the velocity obtained in the hard rock section of the VSP for the pressure wave, with the sonic averages we calculated in the previous chapter. The P-wave velocity displayed on Figure 5.4 corresponds to a quadratic fit of all the picked times, and thus gives a good approximation for the changes in velocity at the scale of the borehole. Figure 5.6 shows that this P-wave velocity (labeled polynomial) is a good trend for the sonic, but obviously does not represent velocity variations on the same scale as the sonic do. Sonic measure the P-wave velocity using very high frequency tools (around 20 kHz), while the frequency band for seismic wave here is about 30 to 140 Hz. Hence we derived more local P-wave velocities, by inversion of the arrival times using a damped least square minimization, and by fitting a local slope of several successive times. Both curves agree well with the previous polynomial fit, showing a P-wave velocity increasing with depth. They also show local variations, matching with the sonic in the deepest part (below 340m). Usually sonic have higher velocities than seismic measurements. This is the case here in the deepest part again (below 340 m), while in the middle (between 300 and 340 m) all the velocities agree with each other, and in the top part (from 240 to 300 m) the sonic velocities mostly seem to be slower than the seismic velocities. Porosity being the main parameter controlling compressive wave velocity, these observations may be related to the degree of porosity in the rocks. We will develop this idea further in the last chapter.
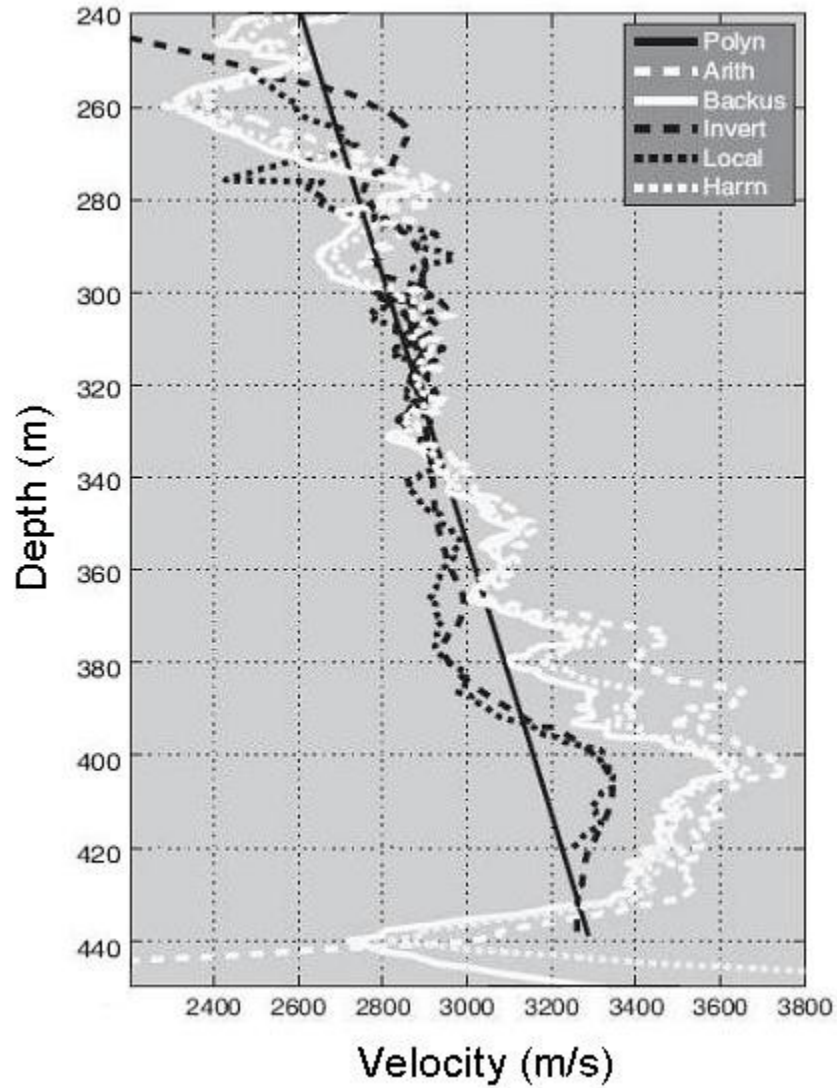
Figure 5.6: Comparison of sonic averages and VSP velocity for the pressure wave. White curves are the different sonic averages (Arith: arithmetic average, Backus: Backus average, Harm: time harmonic average), while black curves are different trends obtained from the VSP times (Polyn: polynomial fit, Invert: inversion of the arrival times, Local: local slope of the picked times)

Chapter 6

Core Studies

6.1 Petrology and Mineralogy

We selected half dozen samples from boreholes LB-08A and LB-07A, representing the various lithologies, and we performed a set of measurements and imaging techniques on them in order to get an idea about their petrography and mineralogy, and to look for probable cracks and characterize them.

6.1.1 X-ray Analysis

X-ray analysis of the samples shows that a few minerals are constitutive of the main types or rock that can be found in the crater. All greywackes contain quartz, calcite, albite and micas. Some greywackes were transformed under pre-impact fluids circulation and contain so much calcite and dolomite that they can actually be called carbonates (Appiah, 1991). Breccias and suevite are mainly made of clasts of greywacke and phyllites, with the matrix being a mix of very small quartz and calcite grains, as can be seen further in the thin section analysis. Phyllites are mainly made of micas; however some traces of quartz and calcite are found.

Micas found here are mainly muscovite and paragonite. these minerals are often the result of the alteration of other minerals under the action of hydrothermal fluids. These minerals are also found in the country rocks surrounding the crater, and this alteration process is known to have occurred before the impact (Karikari et al., 2007).

Another phyllosilicate is found in significant quantities: clinochlore. Ferrière et al. (2007) showed that this alteration into clay minerals was probably post-impact. The presence also of post-impact secondary muscovite was shown by Petersen et al. (2007). This is very likely due to the network of fractures in the crater zone allowing for hot fluids to circulate after the impact.

6.1.2 Thin Sections

Prior to cutting the samples for making thin sections, we impregnated them with a blue dye. This allows us to more easily document the connected porosity when analyzing the thin sections under the microscope.

Figure 6.1 shows a sample of phyllite. We can see a network of cracks of differing widths. They appear to be blue, which means they are connected to the surface of the sample and they account for the porosity of this sample. The rest of the sample does not seem to have any porosity, which is expected for this type of rock. We can compare with Figure 6.2 where the entire matrix of the sample is blueish. We can infer that this sample of carbonated greywacke has a very porous matrix. Same is observed for breccias and suevites. No cracks are visible at the microscope scale, but we can expect a high porosity in our later measurements. The observed opaque minerals are likely to be oxides formed by the hydrothermal alteration.

Greywacke samples often display veins of calcite or quartz. Figure 6.3 shows one of these veins of calcite, in both polarized light and cross-polarized light. We can observe grains of quartz, albite and micas around the vein. This type of veins are most often former cracks now filled up with minerals. The nature of these minerals is gives direct information about the chemical composition of the fluids that once circulated there.

Greywacke samples display some shocked quartz with decorated Planar Features as shown on Figures 6.4 and 6.5. We did not find any ballen quartz, which is consistent with the detailed study of Ferrière et al. (2007). On Figure 6.5 notice cracks within the crystal of quartz and probable zones of recrystallization.

Figure 6.6 shows a melt particle that has been partially devitrified. A blueish

43

matrix can be observed around the particle. Melt particles are seldom within the crater but can be found in some shallow breccias/suevites, like this one from the upper open section of borehole LB-07A.

Figure 6.1: Sample of phyllite in polarized light. Width of microscope field: approximately 5mm.

Figure 6.2: Sample of a carbonated greywacke in polarized light. Width of microscope field: approximately 5mm.

45
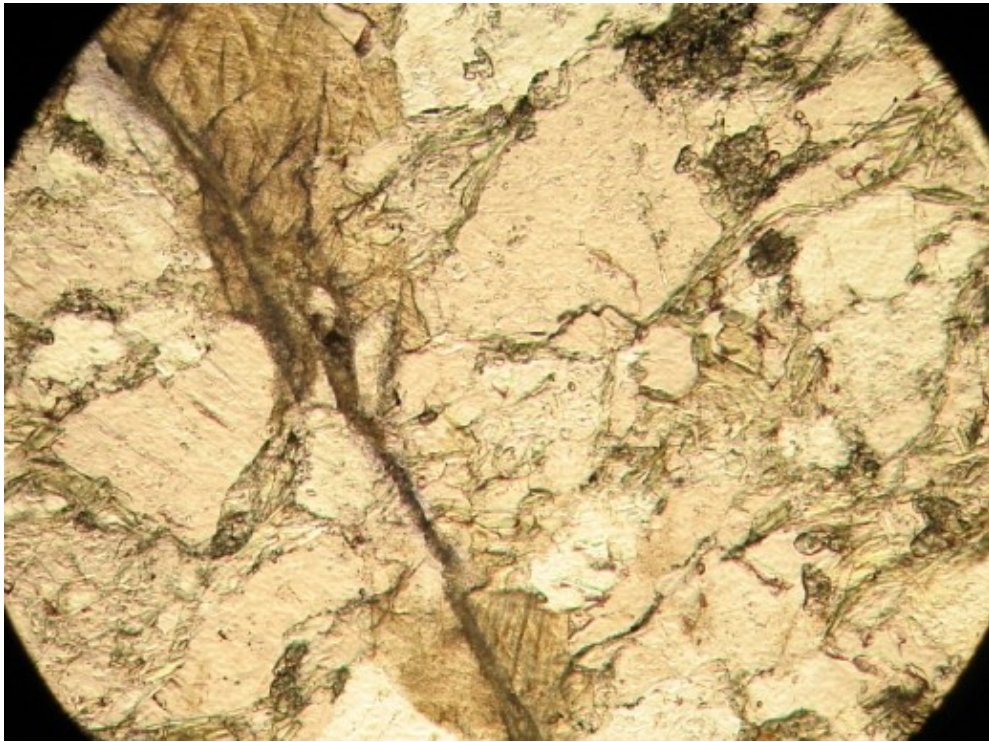
Figure 6.3: Sample of greywacke in polarized (upper panel) and cross-polarized light (lower panel), with a calcite vein running through it. Width of microscope field: approximately 5mm.

Figure 6.4: Quartz grain exhibiting decorated Planar Features in polarized (upper panel) and cross-polarized light (bottom panel). Width of microscope field: approximately 5mm.

Figure 6.5: Quartz grain in a greywacke, with PFs and cracks. Also some parts of the crystal on the left side seem to have recrystallized. Width of microscope field: approximately 5mm.
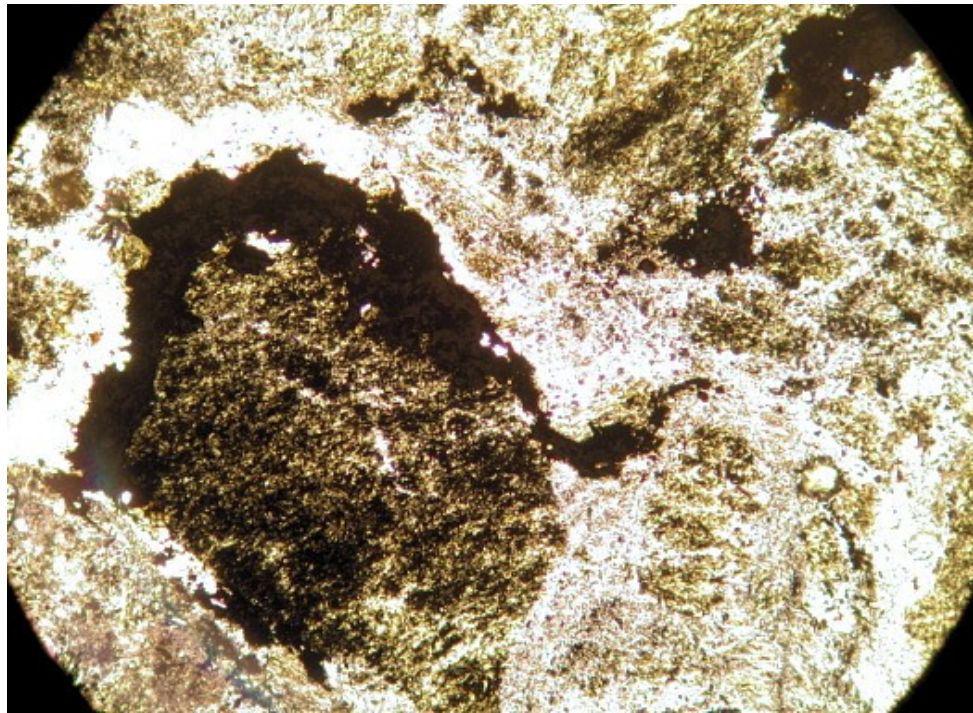

Figure 6.6: Melt particle in a suevite sample, with vitrified (or glassy) and devitrified portions. Width of microscope field: approximately 5mm.

6.1.3 Scanning Electron Microscopy

The SEM technique allows surface imaging to a much smaller scale than usual optical microscopes are capable of. We used the JEOL 6301F type microscope installed in the Earth and Atmospheric Sciences Department building, at the University of Alberta, to look for microcracks and other micron scale features on the minerals. The microscope is also equipped with a PGT X-ray microprobe which is convenient for analyzing the chemical composition of the observed crystals.

Numerous microcracks can be seen in the greywacke samples (Figure 6.7). It is noticeable that most of them are around 1 μm wide. Figure 6.8 displays the same type of microcracks in a quartz grain of another greywacke sample, but with some calcite grains present along these microcracks.

In Figure 6.9 we can see a grain of quartz with a very dense network of microcracks. These cracks are a bit smaller than what we observed in the two previous samples (a tenth of a micron in width).

Figure 6.10 exhibits very unusual geometry and features. It seems that the lower and smaller quartz grain is pushing up like an edge into the upper and bigger quartz grain. Patterns of fractures can be seen around this edge and look like the result of a mechanical strain.

Figure 6.11 shows a set of parallel lines on a quartz grain. They are the same as the Planar Features visible on the thin sections. Another grain displays two sets of PFs (Figure 6.12). One of these sets actually looks like cracks of about one micron width.

All these microcracks and Planar Features are not normally found in rocks. Very high pressures are required to damage minerals in this way, as described in the first chapter.
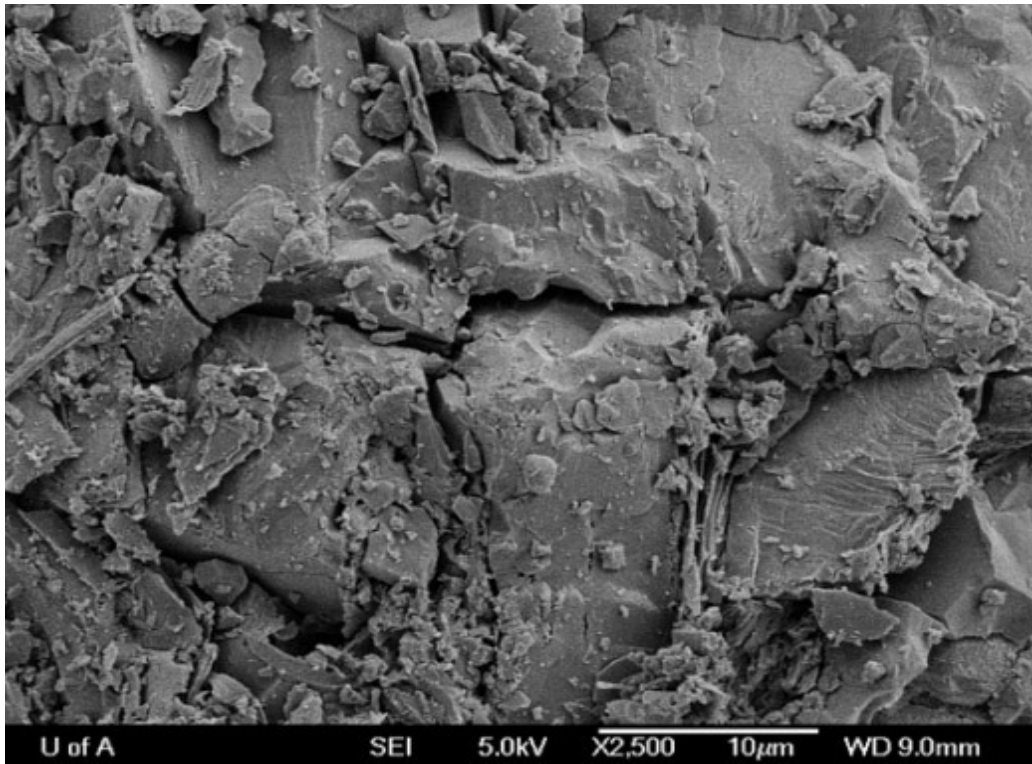
Figure 6.7: Greywacke sample displaying microcracks approximately 1 micron wide.
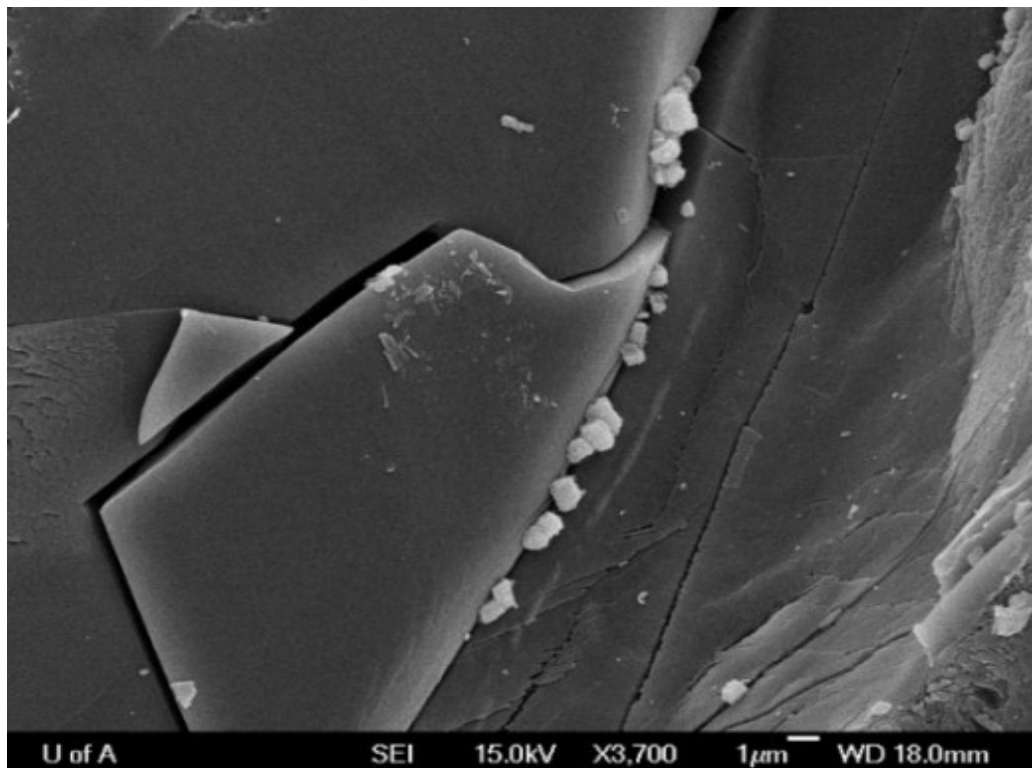
Figure 6.8: A microcrack in a quartz crystal with small calcite grains in it.
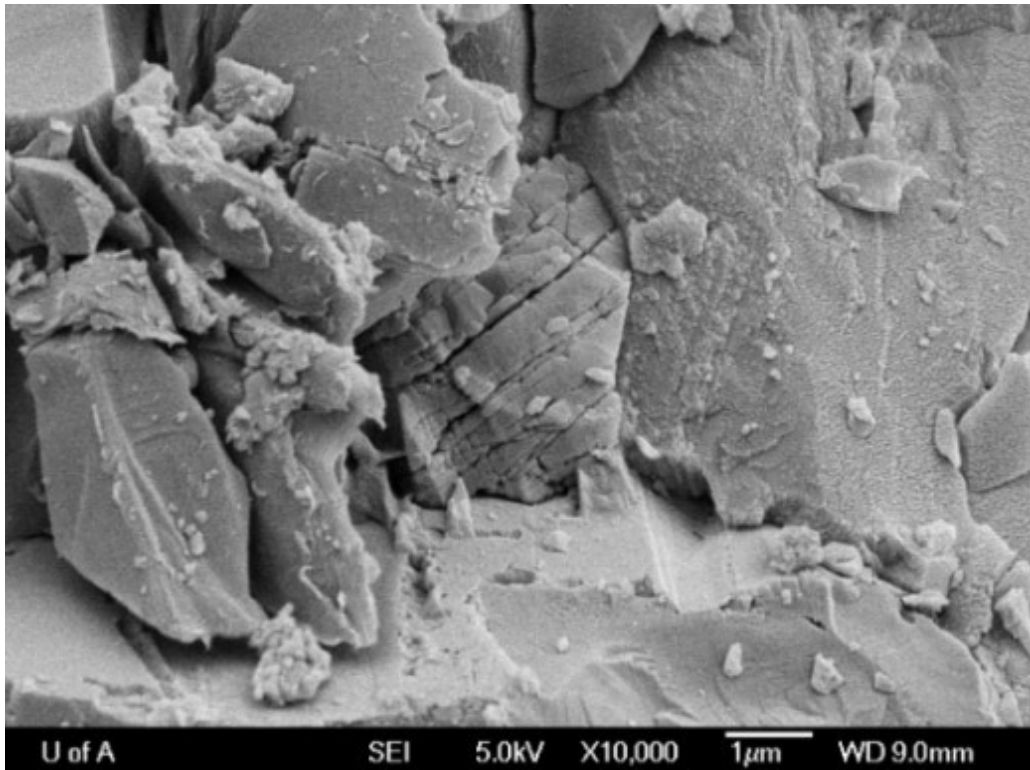
Figure 6.9: An intensely fractured quartz grain in a greywacke sample.
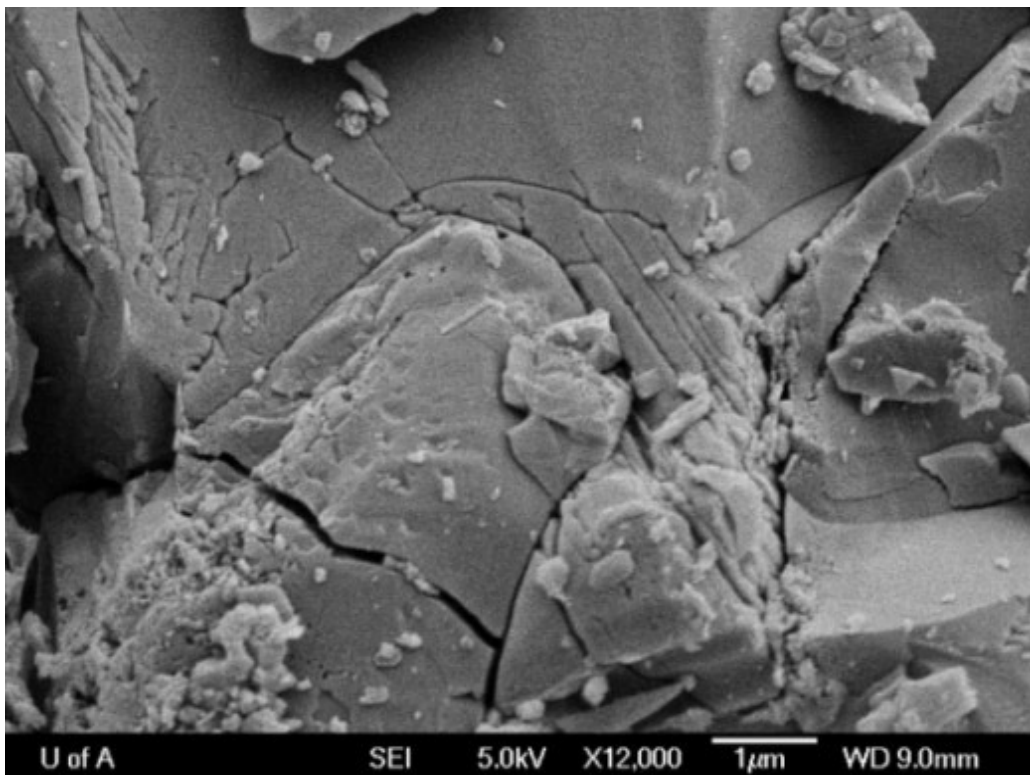
Figure 6.10: Interesting fracture patterns at the contact of two quartz grains.
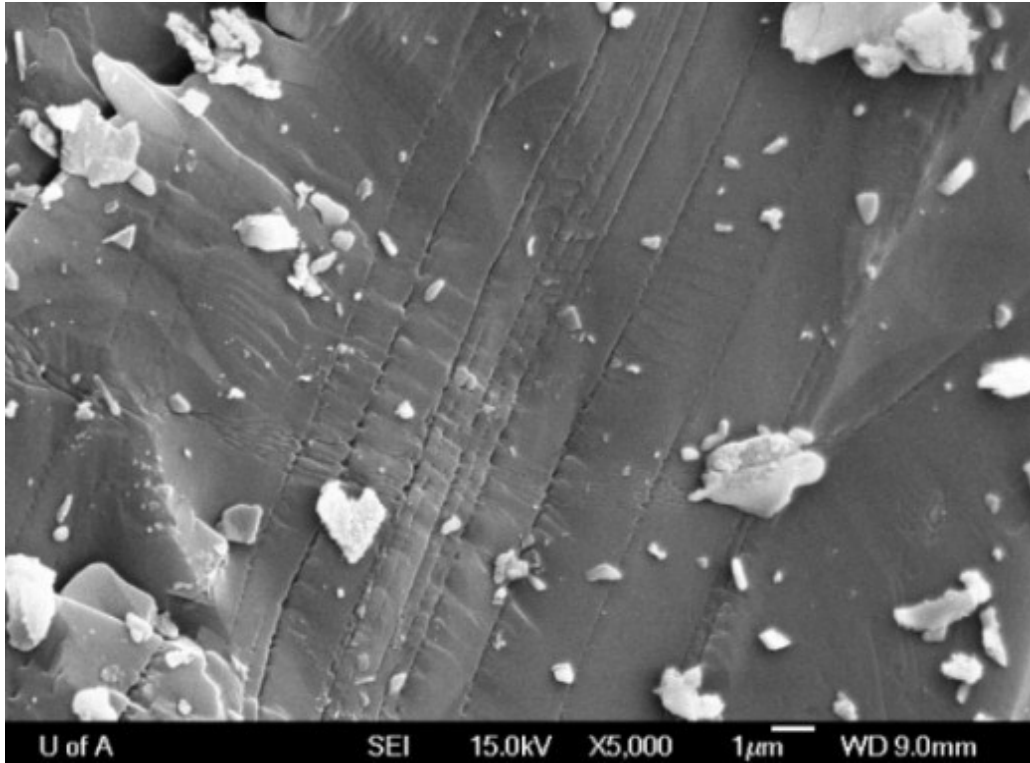
Figure 6.11: Planar Features in a greywacke quartz crystal.
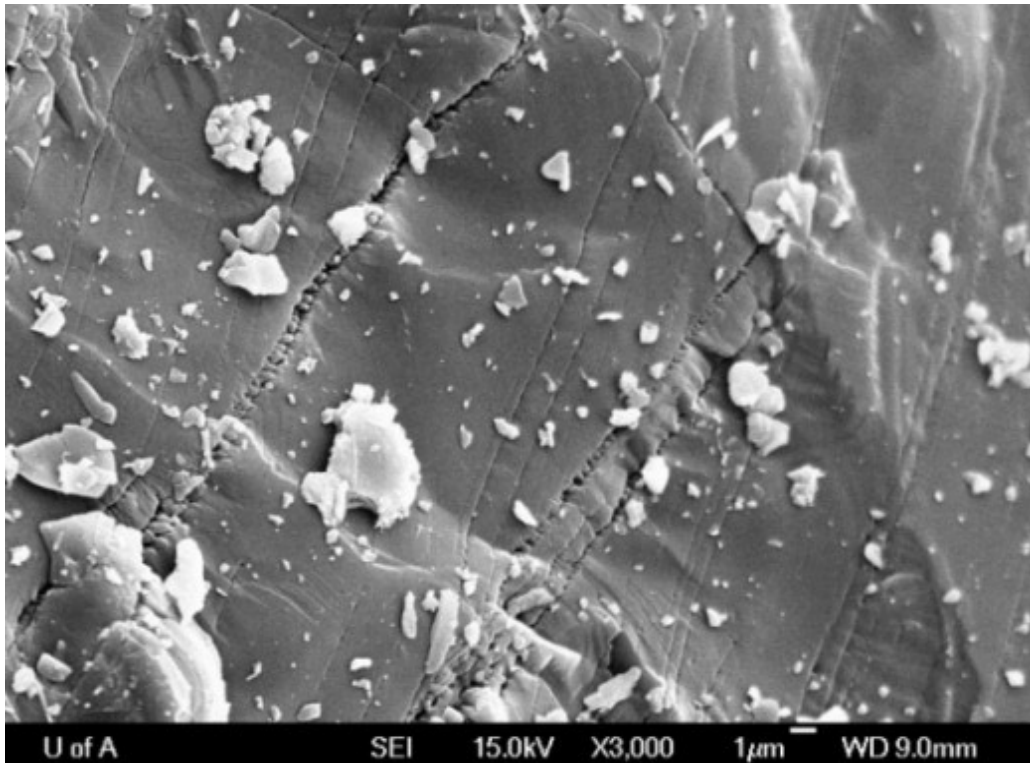
Figure 6.12: Two sets of PFs in a quartz grain. One set of cracks are 1μm wide.

6.2 Physical properties

Porosity, envelope density and grain density were measured on 90 rock samples from deep boreholes LB-07A and LB-08A. Additionally, mercury porosimetry was done on a dozen samples.

6.2.1 Densities and Porosity

The samples were weighed before and after being put in a desiccator in order to monitor the mass change and make sure they are not altered. The volume of the dry samples was accurately determined using a Micrometrics Geopyc envelope density analyzer. Ultimately, a He-pycnometer is used to measure the porosity of the sample. these parameters gathered, simple calculations give us the bulk (envelope) density and the grain density of the samples.

Results yield grain densities ranging from 2.65 g/cm^3 to 2.8 g/cm^3 (Figure 6.13), which is consistent with the silicate minerals identified earlier. Envelope densities are more variable, ranging from 2 g/cm^3 to almost 2.8 g/cm^3. This is due to large variations in the porosity from 1% to nearly 40%. When plotting porosity versus envelope density (Figure 6.14), a linear relationship is seen. This was expected given the narrow range of grain densities.

We can see from Figure 6.15 that there is no obvious relationship between porosity and depth. However a bimodal clustering of the porosity is observed, with a first group of samples between 1% and 9% and a second one between 16% and 24%. The first group contains exclusively samples of phyllites and greywackes. The second one consists mostly of breccias, suevites, and highly fractured or even comminuted greywackes and phyllites.

6.2.2 Mercury porosimetry

This is a destructive technique but a great deal of information can be obtained from it. Pore throat sizes and their occurrence are estimated, which in the end

allows to distinguish between the different pore types within a sample. Pores greater than 100 μm are not analyzed using this technique, but we have to keep in mind from thin sections analysis that millimetric cracks are present in the samples and that they contribute to the overall porosity of the sample.

Figure 6.16 displays the curves obtained for six samples of different lithologies and from different depths. If we assume a theoretically Gaussian distribution of one population of pores in a single sample, then it is an acceptable approximation to say that the pores have a mean size of 1 μm in every sample. These samples have very different lithologies and porosities and surprisingly have the same type or pores. Hence we can infer that all the pores have a common origin, posterior to the original diagenesis.
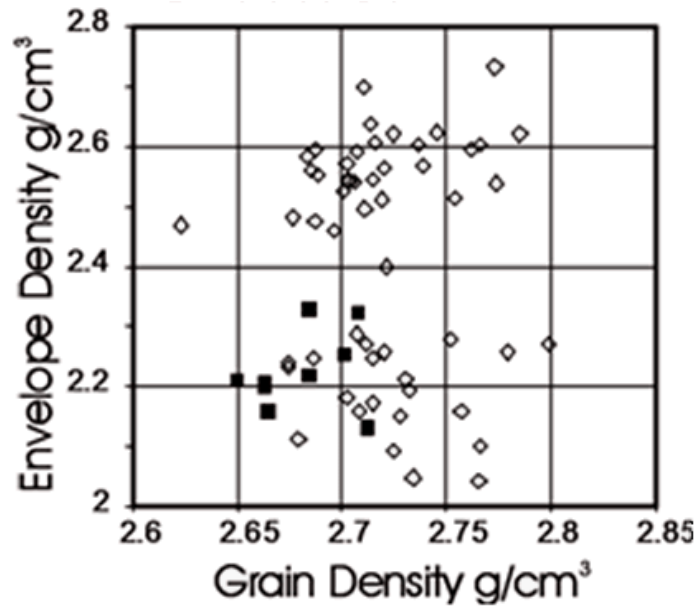
Figure 6.13: Envelope density versus grain density. Squares are surface samples and diamonds are core samples.
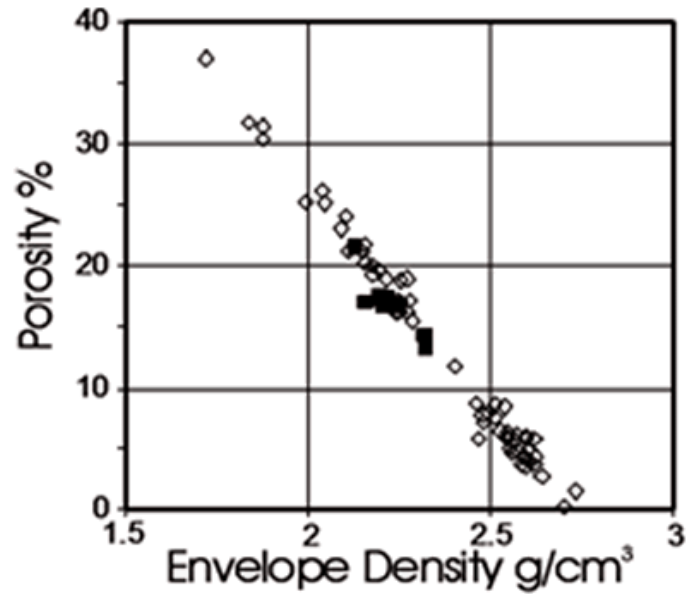
Figure 6.14: Porosity versus envelope density for 90 core samples from holes LB-07 and LB-08.
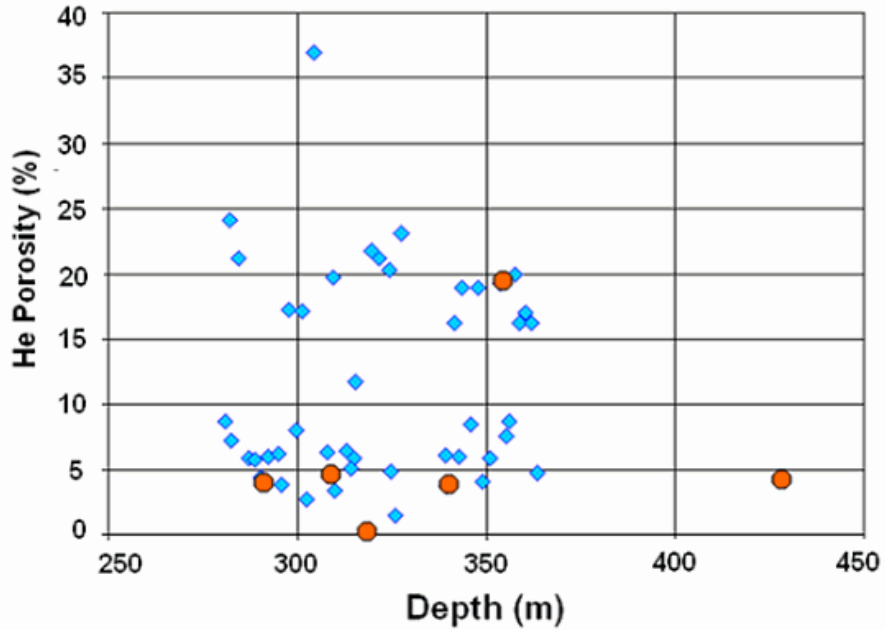
Figure 6.15: He-porosity as a function of depth. Red samples are the ones used for porosimetry display on Figure 6.16.
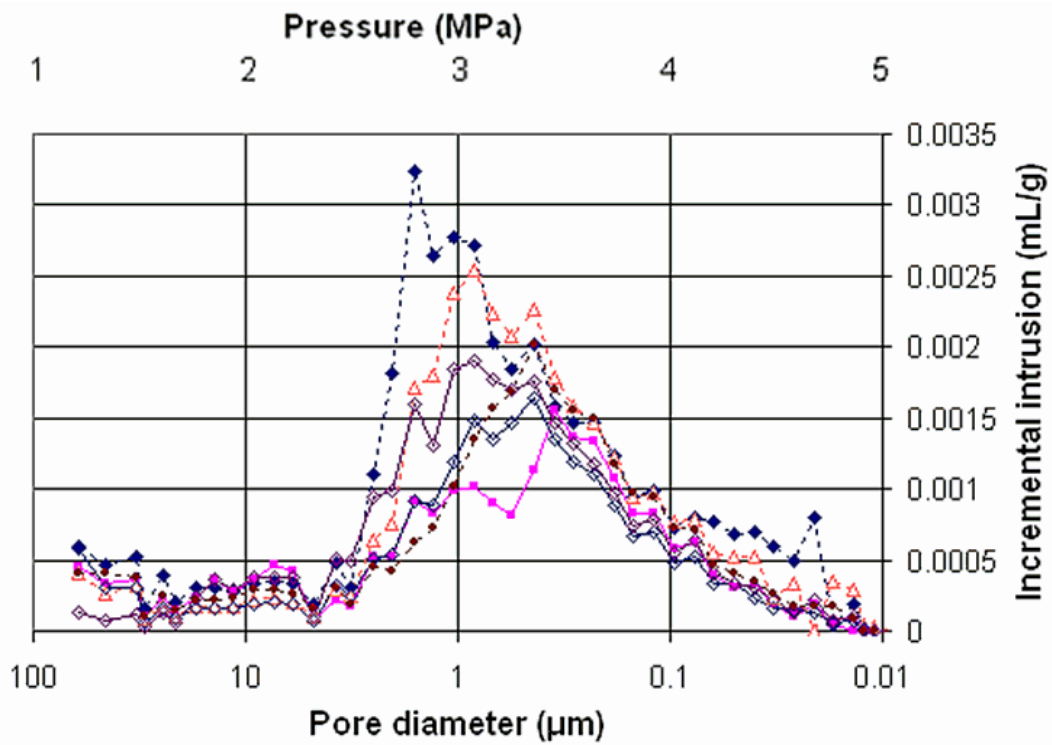
Figure 6.16: Mercury porosimetry results for 6 samples of various lithologies: 2 greywackes, 2 phyllites, 1 carbonate, 1 breccia.

6.3 Velocity measurements

We measured the velocity of P and S waves as a function of pressure through the rock samples, using the pressure vessel of the rock physics laboratory at University of Alberta (Cholach et al., 2005).

Prior to measurements the samples have to be cut and polished. Due to the highly damaged state of most of the rocks (numerous cracks and microcracks), some of them broke during the preparation. Despite the problems occurring while working with such materials, however, a sample for each main lithological facies was obtained.

6.3.1 Carbonate

Two cycles of measurements were performed on the sample, with pressures ranging from 2.5 MPa to 17.5 MPa, and a step in measurement of 1.5 MPa while increasing then decreasing confining pressure. Results are presented on Figure 6.17 and show a hysteresis that is very common in such measurements (Cholach et al., 2005). Velocity values are greater when pressure is decreasing than when it is increasing. This can be explained by a lack of relaxation of the rock since it is still confined and under pressure. For the first cycle, at very low pressures, the opposite happens: last velocities (decreasing) are below the first ones (increasing). The weak sample has probably been damaged at higher pressure and lost some of its original cohesion.

P wave velocity increases from 1800 m/s to 2080 m/s and S wave velocity from 900 m/s to 1080 m/s, which are lower than what is expected for this type or rock, when undamaged. Figure 6.18 shows the corresponding waveforms.

6.3.2 Greywacke

Three cycles were performed with a pressure step of 1 MPa. Starting at 1 MPa, the maximum pressure was increased for each cycle: 10, 20 and 25 MPa respectively. For the P wave during the first cycle, no relationship between velocity and pressure is observed (Figure 6.19). For the second and third cycles,

we can see a trend, with a slight increase of the velocity from 3920 m/s to 3960 m/s. The behaviour is the same for the S wave, with a flat curve for the first cycle and then an increase of velocity with pressure for the two other cycles. On the first cycle, we probably stayed at too low pressures to be able to observe this increase clearly. This may also be due to compaction of the rock during the first cycle. Hence the non-compacted rock did not respond to the increase of pressure in terms of wave velocity. Though the greywackes have been moderately metamorphosed (pre-impact) in our case, we can notice that these P and S waves velocities are in the usually observed range for unmetamorphosed greywackes.

Moreover, for the second and third cycles, the S wave velocity shows some big "steps". Strikingly the repeatability is very good, with the first step occurring around 18 MPa when increasing pressure, and the second step occurring around 10 MPa when decreasing pressure, for both cycles. An hypothesis would be that the opening and closing of a crack in the sample suddenly decreases and increases the velocity, respectively.

6.3.3 Phyllite

As expected Figure 6.20 shows an increase of P wave velocity with pressure, starting at 3200 m/s to get quickly around 3400 m/s (at 5 MPa), and then reaching a maximum of 3600 m/s (at 18 MPa). This is expected P wave velocities for shales.

It was very hard to get a strong signal for both P and S waves in this sample, and unfortunately this latter could not be picked, the seismic trace being too noisy.

6.3.4 Impact Breccia (polymict)

Due to technical problems, we could gather good data on the breccia sample only for one cycle. We can see on figure 6.21, for both P and S waves, the same hysteresis as was seen for the carbonated sample, with higher velocities on the way down, except for the final measurement that falls below the curve once again.

P wave velocity increases from 2350 m/s to 2550 m/s (with a final downgoing velocity of 2000 m/s), while the S wave increases from 1340 m/s to 1460 m/s. Since –to our knowledge- this is the first time such measurements are made on this type of rock, we have no reference to compare these velocities with.
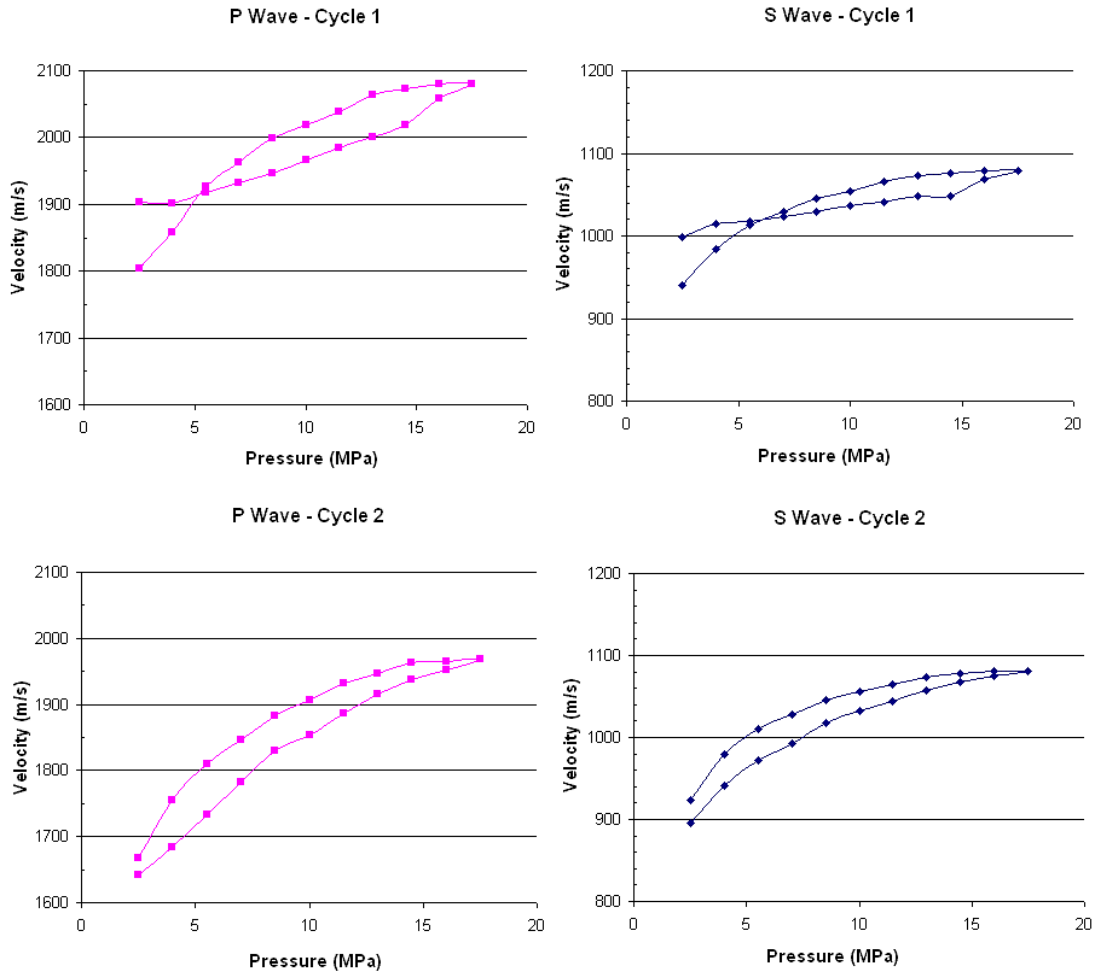
Figure 6.17: P and S waves velocity measurements for a carbonate sample, for two consecutive cycles. Starting pressure is 2.5 MPa, and maximum pressure is 17.5 MPa, with a step of 1.5 MPa between measurements.
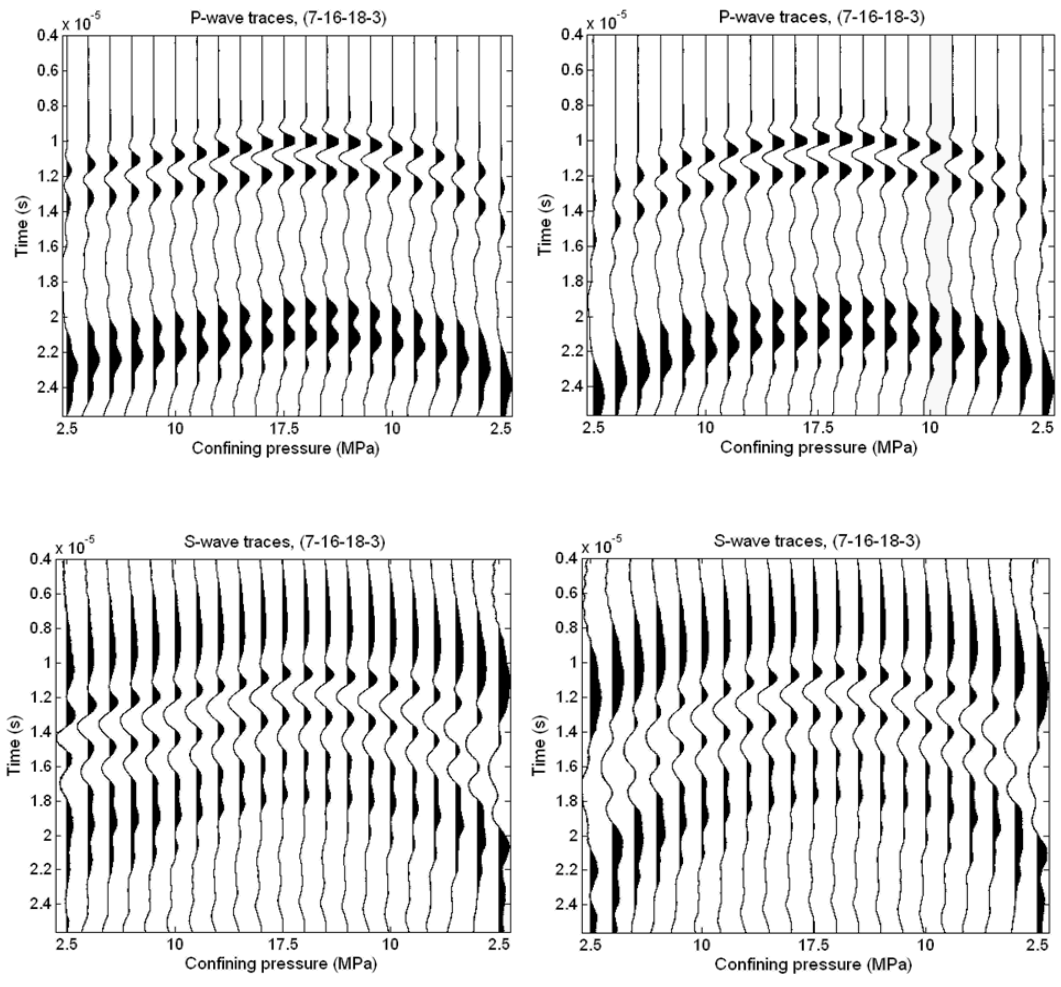
Figure 6.18: Waveforms for P and S waves in the same carbonate sample as in Figure 5.17.
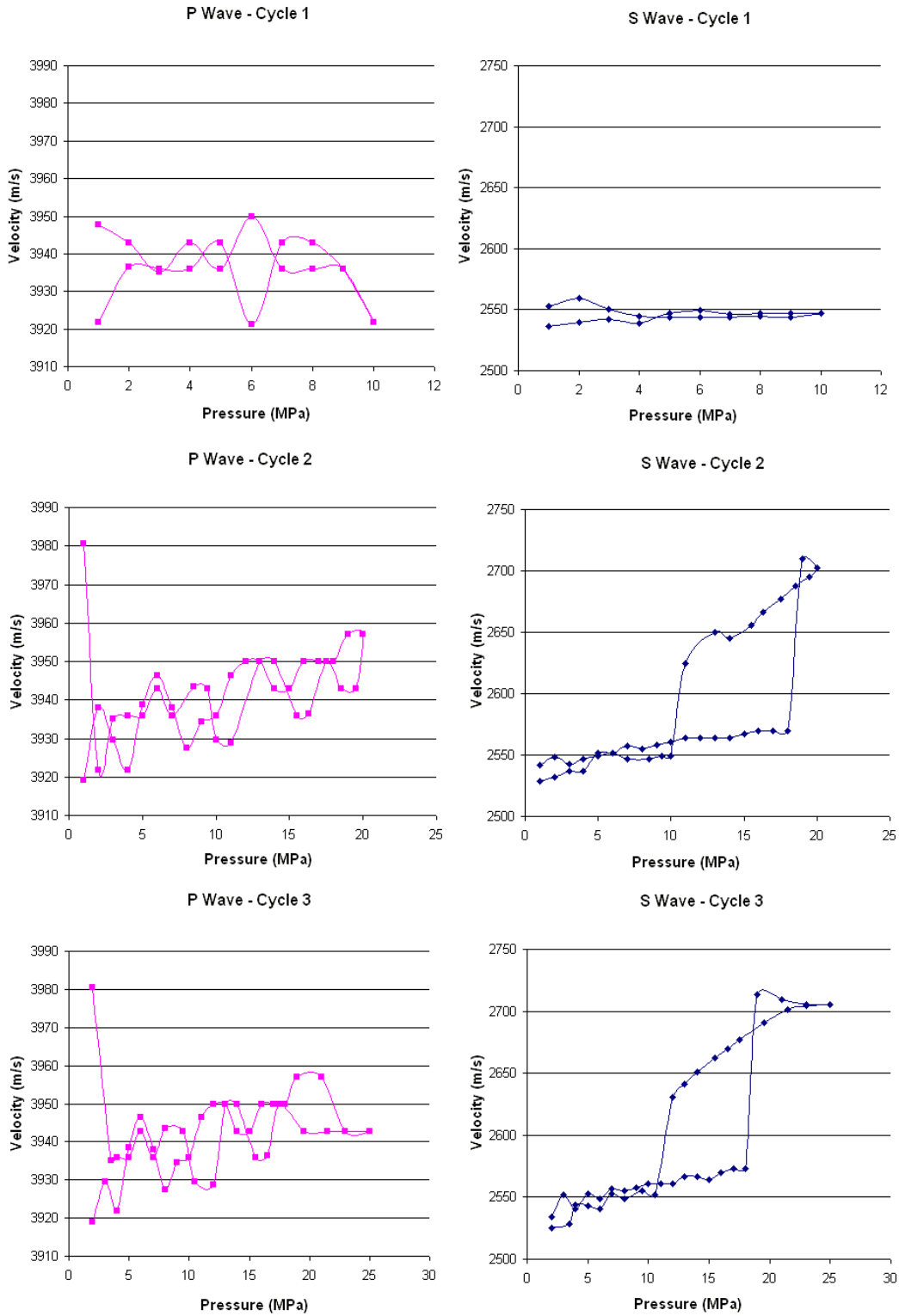
Figure 6.19: P and S waves velocities for a greywacke sample, for three consecutive pressure cycles, with an increasing maximum pressure of respectively 10 MPa, 20 MPa, 25 MPa.
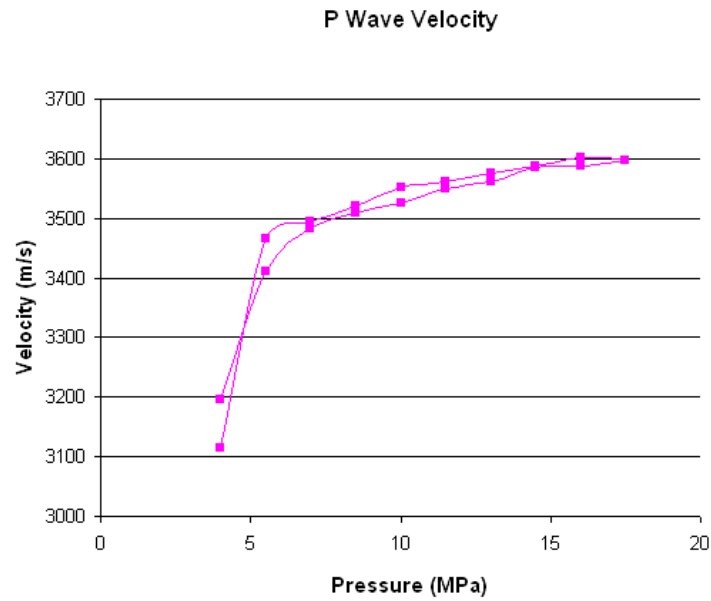
Figure 6.20: P wave velocity in a phyllite sample. First measurement for a confining pressure of 4 Mpa; maximum pressure of 17.5 Mpa; with a step of 1.5 MPa.
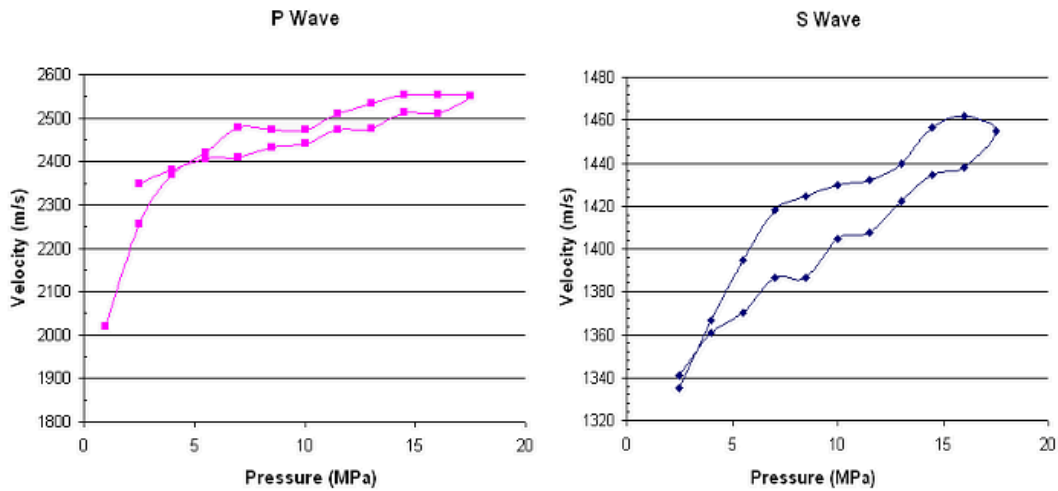
Figure 6.21: P and S waves velocities for a breccia sample. First measurement for a confining pressure of 1 Mpa; maximum pressure of 17.5 Mpa; with a step of 1.5 MPa.

63

Chapter 7

Interpretation

7.1 Macrocracks

As discussed earlier, results by Koeberl et al (2007) and Hunze and Wonik (2007) show that televiewer data are hard to interpret. It is impossible to tell if the observed open fractures are pre-impact structures, impact related structures, or consequences of the drilling. The only reliable data is the unusual very high density of fractures observed, which in regard to the environment of this study can be seen as a clue for impact induced fractures into target rocks, and a random distribution of these fractures into both impactites and target rocks.

A structural geology study by Reimold and al. (1998) shows an intense thrust faulting of multiple orientations within the crater. Our thin sections show veins of quartz and calcite. Once again it is hard to distinguish if these cracks were filled before or after the impact. According to Appiah (1991), crystallisation of carbonates and quartz occurred a long time before the impact. Karikari et al. (2007) show that a later circulation of fluids altered impact glasses and melt particles into argillaceous minerals. Hence it is likely that most of the observed quartz and calcite veins formed before the impact. However there are indications of hydrothermal fluids circulation after the impact as well.

Our lab measurements showed that millimetric or centimetric open cracks account a lot for the porosity of some samples (especially phyllites) and the

distribution of these cracks is random and heterogeneous.

7.2 Microcracks

Our mercury porosimetry measurements showed that pores are of similar size in all the samples. We can deduce that all the pores in the different rock types have a common origin and hence that the different lithologies were affected by the same process. From mercury porosimetry pore size is typically between 0.3 μm and 2 μm. This is too large to be interpreted as the natural structural porosity of the rock (inter-grain porosity). This size is typical for microcracks (French, 1998), which were seen also on our SEM imaging in different rocks, often exhibiting a width of around 1 μm. All these clues lead to confirm the existence of an impact-induced micro porosity in all the different types of rock within the crater.

From the in situ sonic measurements, Hunze and Wonik (2007) noticed that shales and greywackes have the same velocities, while breccias show lower velocities. From our laboratory measurements we found that the breccia sample has lower P-wave velocities than the two other lithologies. This is to be linked with our porosity measurements, where we observed higher porosities in the core samples of suevite and breccia than in the greywackes and phyllites. This can be explained by the high porosity of the matrix of these rocks, as seen in our thin sections. The interpretation of this is unclear. It may be related to the degree of consolidation of the rock. To answer these questions a systematic microscope study of the core samples is required.

Our comparison of in-situ sonics and seismic P-wave velocity shows that at shallow depths sonic velocities are slower than the seismic velocities, which is unusual. But deeper in the wellbore the sonic wave speeds are faster than the seismic. Given the scale we are looking at, sonics may be more sensitive to the density of microcracks. Then the faster increase of sonic velocity with depth

65

compared to the slower seismic velocity increase could be explained by a decrease in the density of microcracks. Our lab measurements on core samples did not show any relationship between porosity and depth, but rather large variations of the porosity for the same type of rock or at the same depth. These measurements take into account only the connected porosity -i.e. closed microcracks are not seen. SEM and thin section studies showed that cracks can affect some grains and not others (and then not be connected to each other), and that late crystallization occurred in some microcracks (due to post-impact fluid circulation). Hence while porosity measurements may not see a significant part of the microcracks, the change in the ratio of sonics and seismic velocities may be an indicator of the change in true porosity.

Assessing the degree of micro fracturing is of primary importance since very high porosities have consequences for the mechanical stability of rocks, and thus for the long-term evolution of the impact structure. Faults and folding seen in the sediment fill on the reflection seismic section witness post-impact motions within the crater. This may indicate a differential compaction and/or fracturing of the impactites (Scholz and Karp, 2007).

7.3   Seismic velocities and heterogeneity

Velocities in the greywacke core sample are the same as in the non-damaged protolith (although this assumes the material has not been significantly metamorphosed), while velocities in the carbonated greywacke and the shale are somehow lower. Impact breccias are formed by definition during impact events; then of course there is no protolith to which they might be compared. Lower than normal velocities were expected in our samples, as impact damaged rocks never recover their original elastic properties (He and Ahrens, 1994). Then the only surprising result is the high velocities in the greywacke sample. We should keep in mind that among the 90 core samples we had, only a few of them were suitable for velocity measurements in the lab, and most probably the less damaged ones. Moreover two greywacke samples broke during the preparation. So the one we

measured on is very likely to be more consolidated (less damaged), which logically induces higher seismic velocities.

Given the complex geology of the crater structure, it is possible to find material of the size of our samples that was almost not affected by the impact. Collins et al. (2004) made a numerical model of a mid-sized impact (10 km crater) into a brittle material (granite). these parameters are likely similar to the Bosumtwi impact case. Results show that strain (i.e. damage) is very heterogeneous at a block scale (decimetric to metric) in a brittle material, but is also consistent with an average smooth strain on a larger volume of rock. This can be interpreted as possible large variations in the degree of damage from one core sample (a few centimeters across) to another. In other words it is possible to find material of the size of our samples that was remained nearly undamaged by the impact, and this can explain the variable results of our core lab measurements. Finally the modeling indicates that the total accumulated strain should correlate with global variations in bulk density and seismic velocities (when total strain increases, density and seismic velocities decrease). Furthermore L'Heureux and Milkreit (2007) show that impactites, though geologically defined as a heterogeneous medium, are homogeneous at the seismic scale, which is consistent with the previous modeling as well as our VSP results.

New results from magnetic and gravity fields modeling concede that the impactite fill of the crater is more heterogeneous that what was expected. The predicted melt layer (Plado et al., 2000) was not hit by the drillings, and a new model from Ugalde (2007b) using in-situ borehole magnetic measurements indicates a patchy distribution of impact melts within the crater. Gravity modeling (Ugalde et al., 2007a) demonstrate lateral density variations within the impactites crater fill, which means changes in porosity and/or rock types. All this is in agreement with our work and with the aforementioned petrophysical and seismic studies.

Chapter 8

Conclusions and Future Work

Our integrated study of the Bosumtwi impact crater included downhole seismic (VSP) and sonics from the field, petrophysical parameters measurements on core samples in the lab, thin section and X-ray analysis of these samples, interpreted in the context of the crater and local area geology previously described by various authors.

We revealed lower than expected velocities for the VSP, the sonics and the laboratory measurements in the different types of rock. These low velocities are usually explained by high porosity, i.e. in our case cracks into the impacted rocks. However no cracks were detected from our VSP study. Hence core sample analysis was required to identify these expected cracks. We also saw that the comparison of sonic and seismic velocity behaviour may indicate the relative density of cracks. In our case sonics are probably more affected by changes in the density of the microcracks than by changes in the lithology. We also noticed small scale heterogeneity in our core samples. Due to the highly damaged state of the samples, we were very limited on the number of samples suitable for lab measurements. It would be best to have regularly and densely spaced drill core samples for all the lithologies, in order to get statistics for the velocities and assess the small scale heterogeneity of impact damaged rocks. Similar studies in the future should take this point into account prior to any field work.

The core sample study revealed that the porosity was higher than expected for undamaged rocks, going up to 40% for some samples. Macrocracks account a lot for these extreme values. For other samples, micrometric porosity is prevalent.

We showed that the high porosities in impact damaged target rocks and impactites were due to a network of microcracks in the matrix. We characterized the average size (1 micron) and the distribution of these cracks through mercury porosimetry in our laboratory and SEM investigation of the core samples. We also concluded the unique origin of these microcracks in all the rock types, i.e. the impact event. Understanding why the matrix has a higher porosity than the original clasts is probably a key in understanding the consequences of the impact on the rocks. Is it related to the degree of consolidation of the

rock? To answer these questions an extended and systematic microscope study (SEM and

thin sections) on a great number of rock samples is required.

As we see the crater fill is much more complex than what was expected, in terms of geology and of petrophysical properties. It is hard to link any lithology to specific physical values, mainly because of the high degree of heterogeneity in the damage and porosity of the rocks. Only integrated studies taking into consideration data from the mineral scale to the crater scale will allow us to truly understand the formation and evolution of such complex geologic objects as impact craters.

Bibliography

Ai H. A. and Ahrens T. J. (2004), *Dynamic tensile strength of terrestrial rocks and application to impact cratering*, Meteoritics & Planetary Science, 39, 233-246.

Ai H. A. and Ahrens T. J. (2007), *Effects of shock-induced cracks on the ultrasonic velocity and attenuation in granite*, Journal of Geophysical Research, 112.

Alvarez L. W., Alvarez W., Asaro F., and Michel H. V. (1980), *Extraterrestrial cause for the Cretaceous-Tertiary extinction,* Science, 208, 1095-1108.

Appiah H. (1991), *Geology and mine exploration trends of Prestea Goldfields, Ghana*, Journal of African Earth Science, 13, 235–241.

Artemieva N. (2007), *Possible reasons of shock melt deficiency in the Bosumtwi drill cores*, Meteoritics & Planetary Science, 42, 883-894.

Boamah D. and Koeberl C. (2003), *Geology and geochemistry of shallow drill cores from the Bosumtwi impact structure, Ghana,* Meteoritics & Planetary Science, 38, 1137-1159.

Chao E. C. T. (1968), *Pressure and temperature histories of impact metamorphosed rocks – Based on petrographic observations*, in French B. M. et al., eds., Shock metamorphism of natural materials, Monon Book Corp., Baltimore, 135-158.

Cholach P. Y., Molyneux J. B., and Schmitt D. R. (2005), *Flin Flon Belt seismic anisotropy: elastic symmetry, heterogeneity, and shear-wave splitting,* Canadian

Journal of Earth Sciences, 42, 533–554.

Collins G. S., Melosh J., and Ivanov B. (2004), *Modeling damage and deformation in impact simulations*, Meteoritics & Planetary Science, 39, 217-231.

Danuor S. K. and Menyeh A. (2007), *Results of pre-drilling potential field measurements at the Bosumtwi crater*, Meteoritics & Planetary Science, 42, 541-547.

Donofrio R. R. (1997), *Survey of hydrocarbon-producing impact structures in North America: Exploration results to date and potential for discovery in Precambrian basement rock*, Oklahoma Geol. Survey, Circ., 100, 17–29.

Dressler B. O. and Reimold W. U. (2001), *Terrestrial impact melt rocks and glasses*, Earth-Science Reviews, 56, 205-284.

Earth Impact Database (2008), Planetary and Space Science Centre, University of New Brunswick, *www.unb.ca/passc/ImpactDatabase*. (Accessed: december 2008)

Ferrière L., Koeberl C., Reimold W. U. (2007), *Drill core LB-08A, Bosumtwi impact structure, Ghana: Petrographic and shock metamorphic studies of material from the central uplift,* Meteoritics & Planetary Science, 42, 611-633.

Foucault A. and Raoult J.-F. (1995), *Dictionnaire de Géologie*, 3e édition, Dunod.

Free Map Library (2009), Académie d'Aix-Marseille, France, *http://histgeo.ac-aix-marseille.fr/webphp/pays.php?num_pay=23&lang=en*. (Accessed: january 2009)

French B. M. (1998), *Traces of Catastrophe: A Handbook of Shock-Metamorphic Effects in Terrestrial Meteorite Impact Structures,* LPI Contribution 954, Lunar

and Planetary Institute, Houston.

Furukawa Y., Sekine T., Oba M., Kakegawa T., and Nakazawa H. (2009), *Biomolecule formation by oceanic impacts on early Earth*, Nature Geoscience, 2, 62-66.

Hardage B. A. (1983), *Vertical seismic profiling*, Part A, Principles, 1st ed., Amsterdam, Elsevier.

Hayward C. L., Reimold W. U., Gibson R. L., and Robb L. J. (2005), *Gold mineralisation within the Witwatersrand Basin, South Africa: evidence for a modified placer origin, and the role of the Vredefort impact event*; Mineral Deposits and Earth Evolution, Geol. Soc. London, Special Publication, 248, 31–58.

He H. and Ahrens T. J. (1994), *Mechanical properties of shock damaged rocks*, Int. J. Rock Mech. Min. Sci. & Geomech. Abstr., 31, 525-533.

Hunze S. and Wonik T. (2007*), Lithological and structural characteristics of the Lake Bosumtwi impact crater, Ghana: Interpretation of acoustic televiewer images*, Meteoritics & Planetary Science, 42, 779-792.

Isbell W. M. (2005), *Shock waves: measuring the dynamic response of materials*, Imperial College Press, London.

Jones W. B., Bacon M., Hastings D. A. (1981), *The Lake Bosumtwi impact crater, Ghana*, Geological Society of America Bulletin, 92, 342-349.

Karikari F., Ferrière L., Koeberl C., Reimold W. U., and Mader D. (2007), *Petrography, geochemistry, and alteration of country rocks from the Bosumtwi impact structure, Ghana,* Meteoritics & Planetary Science, 42, 513-540.

Karp T., Milkereit B., Janle P., Danuor S. K., Pohl J., Berckhemerd H., Scholze C. A. (2002), *Seismic investigation of the Lake Bosumtwi impact crater: preliminary results*, Planetary and Space Science, 50, 735-743.

Koeberl C., Bottomley R., Glass B. P., Storzer D. (1997), *Geochemistry and age of Ivory Coast tektites and microtektites*, Geochimica et Cosmochimica Acta, 61, 1745-1772.

Koeberl C., Reimold W. U., Blum J. D., and Chamberlain C. P. (1998), *Petrology and geochemistry of target rocks from the Bosumtwi impact structure, Ghana, and comparison with Ivory Coast tektites*. Geochem. Cosmochim. Acta, 62, 2179-2196.

Koeberl C. and Reimold W. U. (2005), *Bosumtwi impact crater, Ghana (West Africa): An updated and revised geological map, with explanations,* Jahrbuch der Geologischen Bundesanstalt, Wien (Yearbook of the Geological Survey of Austria), 145, 31-70 (+1 map, 1:50,000).

Koeberl C., Milkereit B., Overpeck J. T., Scholz C. A., Amoako P. Y. O., Boamah D., Danuor S., Karp T., Kueck J., Hecky R. E., King J. W., Peck J. A. (2007), *An international and multidisciplinary drilling project into a young complex impact structure: The 2004 ICDP Bosumtwi Crater Drilling Project - An overview,* Meteoritics & Planetary Science, 42, 483-511.

Leube A., Hirdes W., Mauer R., and Kesse G. O. (1990), *The early Proterozoic Birimian Supergeroup of Ghana and some aspects of its associated gold mineralization*, Precambrian Res., 46, 139-165.

Liu C. and Arhens T. J. (1997), *Stress wave attenuation in shock-damaged rock*, Journal of Geophysical research, 102, 5243-5250.

73

Lunar and Planetary Laboratory (2009), Department of Planetary Sciences, University of Arizona, *www.meteorites.lpl.arizona.edu/glossary.html*. (Accessed: january 2009)

Lunar & Planetary Institute (2008), Houston, Texas, *www.lpi.usra.edu*. (Accessed: december 2008)

L'Heureux E. and Milkreit B. (2007), *Impactites as a random medium—Using variations in physical properties to assess heterogeneity within the Bosumtwi meteorite impact crater*, Meteoritics & Planetary Science, 42, 849-858.

Melosh H. J. (1979), *Acoustic fluidization: A new geologic process?*, Journal of Geophysical Research, 84, 7513–7520.

Melosh H. J. (1989), *Impact cratering, A Geological process*, Oxford University Press, New York.

Morris W. A., Ugalde H., and Clark C. (2007), *Physical property measurements: ICDP boreholes LB-07A and LB-08A, Lake Bosumtwi impact structure, Ghana*, Meteoritics & Planetary Science, 42, 801-809.

Pati J. K. and Reimold W. U. (2007), *Impact cratering – fundamental process in geoscience and planetary science*, J. Earth Syst. Sci., 116, 81–98.

Pesonen L. J., Koeberl C., Ojamo H., Hautaniemi H., and Elo S. and Plado J., (1998) *Aerogeophysical studies of the Bosumtwi impact structure, Ghana,* Geol. Soc. Amer. Abstracts with Programs, 30, A-190.

Petersen M. T., Newsom H. E., Nelson M. J., Moore D. M. (2007), *Hydrothermal alteration in the Bosumtwi impact structure: Evidence from 2M1-muscovite,*

alteration veins, and fracture fillings, Meteoritics & Planetary Science, 42, 655-666.

Pilkington M. and Grieve R. A. F. (1992), *The Geophysical Signature of Terrestrial Impact Craters*, Reviews of Geophysics, 30, 161-181.

Plado J., Pesonen L. J., Koeberl C., and Elo S. (2000), *The Bosumtwi meteorite impact structure, Ghana: A magnetic model*, Meteoritics & Planetary Science, 35, 723-732.

Pohl, J., Stöffler D., Gall H., and Ernstson K. (1977), *The ries impact crater*, Impact and Explosion Cratering, Pergamon, New York, 343–404.

Reimold W. U., Brandt D., and Koeberl C. (1998), *Detailed structural analysis of the rim of a large, complex impact crater: Bosumtwi crater, Ghana*, Geology, 26, 543–546.

Rio P., Mukerji T., Mavko G., and Marion D. (1996), *Velocity dispersion and up-scaling in a laboratory-simulated VSP*, Geophysics, 61, 584–593.

Schmitt D. R, Milkereit B., Karp T., Scholz C., Danuor S., Meillieux D., and Welz M. (2007), *In situ seismic measurements in borehole LB-08A in the Bosumtwi impact structure, Ghana: Preliminary interpretation*, Meteoritics & Planetary Science, 42, 755-768.

Scholz C. A., Karp T., Brooks K. M., Milkereit B., Amoako P. Y. O., Arko J. A. (2002), *Pronounced central uplift identified in the Bosumtwi impact structure, Ghana, using multichannel seismic reflection data*, Geology, 30, 939–942.

Scholz C. A., Karp T., Lyons R. P. (2007), *Structure and morphology of the Bosumtwi impact structure from seismic reflection data,* Meteoritics & Planetary

Science, 42, 549-560.

Ugalde H., Danuor S. K., and Milkereit B. (2007a), *Integrated 3-D model from gravity and petrophysical data at the Bosumtwi impact structure, Ghana*, Meteoritics & Planetary Science, 42, 859-866.

Ugalde H., Morris W. A., Pesonen L. J., and Danuor S. K (2007b), *The Lake Bosumtwi meteorite impact structure, Ghana - Where is the magnetic source?*, Meteoritics & Planetary Science, 42, 867-882.

Ugalde H., Morris W. A., Clark C., Miles B., and Milkereit B. (2007c), *The Lake Bosumtwi meteorite impact structure, Ghana - A magnetic image from a third observational level*, Meteoritics & Planetary Science, 42, 793-800.

Versh E., K. Kirsimäe K., Jõeleht A., Plado J. (2003), *Impact induced hydrothermal system at Kärdla crater: development and biological consequences*, Large Meteorite Impacts, abstract.

Wright J. B., Hastings D. A., Jones W. B., and Williams H. R. (1985), *Geology and mineral resources of West Africa.* George Allen & Unwin, London.